

Cell surface hydrophobicity determines aggregate assembly type in *Pseudomonas aeruginosa*

Sheyda Azimi¹, Jacob Thomas¹, Sara E. Cleland¹, Jennifer E. Curtis², Joanna B. Goldberg³
and Stephen P. Diggle^{1*}

¹Center for Microbial Dynamics & Infection, School of Biological Sciences, Georgia Institute of Technology, Atlanta, U.S.A.; ²School of Physics, Georgia Institute of Technology, Atlanta, U.S.A.;

³Division of Pulmonology, Allergy/Immunology, Cystic Fibrosis and Sleep, Department of Pediatrics, Emory University School of Medicine, Atlanta, U.S.A.

*Correspondence: stephen.diggle@biosci.gatech.edu

Keywords: Lipopolysaccharide, O-antigen, *Pseudomonas aeruginosa*, cystic fibrosis, hydrophobicity, entropic depletion

Abstract

Bacteria live in spatially organized aggregates during chronic infections, where they adapt to the host environment and evade immune responses and resist therapeutic interventions. Although it is known that environmental factors such as polymers influence bacterial aggregation, it is not clear how bacterial adaptation during chronic infection impacts the formation and spatial organization of aggregates. Here we show that in an *in vitro* model of cystic fibrosis (CF) containing the polymers eDNA and mucin, O-antigen is the major factor in determining the formation of two distinct aggregate assembly types of *Pseudomonas aeruginosa* due to alterations in cell surface hydrophobicity. Our findings highlight that during chronic infection, the interplay between cell surface properties and polymers in the environment determines the formation and structure of bacterial aggregates, and sheds new light on the fitness costs and benefits of O-antigen production in environments such as CF lungs.

Importance

During chronic infection, several factors contribute to the biogeography of microbial communities. Heterogeneous populations of *Pseudomonas aeruginosa* form aggregates in cystic fibrosis airways,

however, the impact of this population heterogeneity on spatial organization and aggregate assembly is not well understood. In this study we found that changes in O-antigen structure determine the spatial organization of *P. aeruginosa* cells by altering the relative cell surface hydrophobicity. This finding provides new insights into the role of O-antigen on the biogeography and structure of *P. aeruginosa* aggregates in cystic fibrosis airways.

Introduction

During chronic infection, biofilm-forming bacteria are often more tolerant to antibiotics and the host immune response than planktonic cells (1-3). Biofilms also allow individual cells the physical proximity to engage in and benefit from social behaviors such as quorum sensing (QS) and the production of secreted common goods (4-9). Biofilms formed during infection often take the form of cellular aggregates which differ from the biofilms observed during *in vitro* growth (8, 10-12). In the fluids of wounds and airways of cystic fibrosis (CF) patients, the opportunistic pathogen *Pseudomonas aeruginosa* frequently grows as freely suspended aggregates of ~10-10,000 cells (6, 8, 10, 11). Aggregates do not need to be surface attached and they provide similar fitness benefits to cells growing in biofilms such as tolerance to antibiotics (13, 14).

Little is known about what governs the shape and size of the aggregates during infection. Studies on bacterial aggregations have suggested that aggregate assembly is either dependent on the physical properties of polymers available in the surrounding environment, where entropic force leads to aggregate formation via a process termed depletion aggregation (15, 16), or electrostatic binding and interaction between negatively charged bacterial cell surfaces with the positively charged polymers in the environment, leading to bridging aggregation (17-20). A study on the aggregation of *P. aeruginosa* suggested that polymers such as mucin and extracellular DNA (eDNA) act as depletants, physically forcing cells together to form aggregates in environments such as CF airways (14). However, the biological factors required for aggregate assembly remain poorly understood.

P. aeruginosa populations become genetically diverse over time in the complex micro-environments found in CF lungs (21-24), and the importance of this heterogeneity on the spatial organization of aggregates has not been assessed. To resolve this, we evaluated aggregate formation in seven genetically diverse isolates sourced from heterogeneous populations of the *P. aeruginosa* strain PAO1 previously

evolved in biofilms for 50 days (25). We grew each isolate in a polymer enriched spatially structured CF growth medium (SCFM2: containing mucin and eDNA polymers), where entropic force was expected to play the main role in aggregate formation (14, 26).

We identified two distinct types of aggregate assembly. The PAO1 ancestor and five isolates formed a stacked pattern (stacked aggregates) where cells closely packed lengthwise into ordered stacks similar to those identified in previous polymer driven depletion-aggregation studies (14). Two isolates formed distinct disorganized clumps of varying sizes (clumped aggregates), similar to the aggregates found in some CF sputum samples (10, 27). In order to identify the underlying mechanism(s) driving the clumped assembly type, we used whole genome sequencing and found that the two clumping isolates had alterations in the *ssg* gene (PA5001). The exact function of *ssg* remains unknown, but previous studies have revealed that it is likely involved in lipopolysaccharide (LPS) and O-antigen biosynthesis (28-30). This observation is a critical clue since changes in the O-antigen can lead to alteration of bacterial surface charge and/or hydrophobicity (31, 32).

We hypothesized that changes in O-antigen structure would lead to different aggregate assembly type by altering the physiochemical properties of the bacterial cell surface that could result in new interactions (e.g. between the bacteria or the bacteria and polymers) that compete with the entropic force that otherwise leads to stacked aggregation in this polymer-rich environment. To identify which component of LPS played a central role in aggregate assembly type, we assessed the aggregate formation of clean mutants of O-specific antigen (B-band, OSA) and common polysaccharide antigen (A-band, CPA). We found that OSA mutants formed clumped aggregates and displayed a higher surface hydrophobicity than wild-type or CPA mutant cells. We also found that clinical isolates of *P. aeruginosa* sourced from CF sputum, displayed a general trend towards an increased cell surface hydrophobicity.

Overall, our findings suggest that *P. aeruginosa* forms distinct types of aggregates in structured (polymeric) environments which are dependent on the LPS O-antigen structure and associated cell surface hydrophobicity. Loss of the OSA and change in the capped LPS core structure alter the cell surface properties, leading to increased hydrophobicity of the cell surface that overpowers the entropic force imposed by host polymers, resulting in disorganized, irreversible clumping. Most importantly, we demonstrate that aggregate assembly is dependent on the interplay between the physical properties of the

environment and the biological mediation of bacterial cell surface properties governed by the LPS core and O-antigen.

Results

Distinct aggregate assembly types in genetically diverse *P. aeruginosa* isolates. Genetic and morphologically heterogeneous isolates of *P. aeruginosa* are commonly collected from expectorated CF sputum samples (22, 23, 33, 34). Since it is known that several lineages of *P. aeruginosa* can stably coexist in CF airways, we tested whether this population heterogeneity impacted aggregate formation. We chose seven distinct morphotypes isolated from a previous study where we evolved biofilms of PAO1 in a synthetic polymer-free sputum media (SCFM) for 50 days (25, 35, 36) (Fig. S1A). We assessed aggregate formation in a spatially structured iteration of SCFM termed SCFM2 which contains mucin and eDNA polymers (26). We identified two distinct types of aggregate assembly, where PAO1 and five of the evolved isolates (A2, B8, B13, C25 and D4) were assembled into stacked aggregates, where cells were closely aligned side by side by entropic force, similar to previous reports (14) (Fig. 1A; Fig. S1B & C). In contrast, two of the evolved isolates (A9, B9) formed clumped aggregates that appeared as disorganized small and large groups of cells, similar to bridging aggregation (17) (Fig. 1A). We also investigated growth of A9 and B9 in SCFM (no addition of eDNA or mucin), and observed that both formed clumps even in a polymer free environment, while the other isolates did not form any aggregates (Fig. S2A).

To identify genetic determinants of clumping assembly in the evolved isolates, we performed whole-genome sequencing on each isolate using the Illumina Miseq platform. We used breseq (0.34.0) for variant calling between the evolved isolates and the PAO1 ancestor (37). Whilst we found differential levels of genetic variation in each isolate when compared to PAO1, we observed that A9 and B9 each contained a 1bp deletion in the *ssg* gene (PA5001) (Dataset 1). To confirm that mutation of *ssg* results in a clumped aggregate assembly, we complemented A9 and B9 with an intact *ssg* gene *in trans*. We found that in both isolates, *ssg* complementation restored the stacked aggregate assembly seen in PAO1 (Fig. 1B; Fig. S2B) suggesting that Ssg plays a role in aggregate assembly type.

A distinct feature of the stacked versus clumped aggregates was the average volume. We found that stacked aggregate volumes were 2-4 times larger (median of $\approx 63 \mu\text{m}^3$ and $89 \mu\text{m}^3$ aggregate size for

PAO1 and A2 respectively) and (median of $\approx 200 \mu\text{m}^3$ in *ssg* complemented A9 and B9) compared to clumped aggregates (median aggregate size of ≈ 23 and $30 \mu\text{m}^3$ for A9 and B9 respectively) (Fig. 1B). To quantify these observed differences in the distribution of aggregate biomass in cells with stacked and clumped aggregate assembly types, we compared the distribution of biovolume (ratio of aggregate volume to surface area) for each type of aggregate assembly in SCFM2. We found that regardless of the size, the median biovolume in stacked aggregates was significantly higher than in clumped aggregates (Table S1).

O-antigen structure and not other biofilm traits determines aggregate assembly type. The proposed function of *Ssg* is a glycosyltransferase, involved in LPS and exopolysaccharide biosynthesis (28, 38). *P. aeruginosa* with mutations in *ssg* have previously been shown to display decreased motility, enhanced phage resistance and to lack O-antigen (28, 30, 39). We next determined whether the different aggregate assemblies due to the loss of *ssg* in our evolved PAO1 isolates was because of differences in O-antigen production. We constructed a clean *ssg* gene deletion in PAO1 (PAO1 Δ *ssg*) and a range of isogenic mutants of glycosyltransferases and synthases of common polysaccharide antigen (CPA or A-band; PAO1 Δ *rmd*), O-specific antigen synthase (OSA or B-band; PAO1 Δ *wbpM*), B-band polymerase (PAO1 Δ *wyz*), and common glycosyltransferase required for initiation of both CPA and OSA to the lipid A core+1 (PAO1 Δ *wbpL*) alongside the ligase involved with attachment of O-antigen polysaccharides to the LPS core (PAO1 Δ *waaL*). In addition, we made mutants in the OSA length regulators (PAO1 Δ *wzz1* and PAO1 Δ *wzz2*) for high molecular weight and very high molecular weight OSA (40, 41) (Fig. S3). We then determined the aggregate assembly type of the O-antigen mutants in SCFM2. We found that *ssg*, *wbpL* and *wbpM* mutants with no OSA, formed clumped aggregates, but lack of CPA (PAO1 Δ *rmd*) did not change the aggregate assembly type (Fig. 2A & B).

Biofilm formation by *P. aeruginosa* is regulated by several well-described mechanisms such as exopolysaccharide production, adhesins and quorum sensing (6, 9, 42, 43). To determine whether any of these factors interfered with stacked aggregation in SCFM2, we examined the aggregate assembly of defined mutants in exopolysaccharide production (PAO1 Δ *pel/psl*), lectins (PAO1 Δ *lecA* & PAO1 Δ *lecB*) and quorum sensing (QS) (PAO1 Δ *lasR*). We found that all these mutants displayed stacked aggregate assembly like PAO1 (Fig. S4). This indicated that changes in aggregate assembly type of A9 and B9 was

not due to alterations in some common phenotypes associated with biofilm formation, only the loss of OSA was important.

Loss of OSA leads to clumped aggregate assemblies independent of polymer and cell density. To determine the differences in stacked and clumped aggregate assembly in SCFM2, despite the presence of polymers, we monitored aggregate assembly of PAO1 and PAO1 $\Delta wbpL$ over time. We found that an increase in initial cell density results in the quick assembly of stacked aggregates, while there was no changes in clumped aggregate assembly (Movie S1 and S2).

When we monitored the aggregate assembly of PAO1 and PAO1 $\Delta wbpL$ over 6 hours, we found that there was a significant change in PAO1 aggregate biovolume after 180 minutes of cells growing in SCFM2 and when the stacks were assembled (Fig. 3A) whereas, regardless of cell density, the biovolume of PAO1 $\Delta wbpL$ aggregates remained constant over time (Fig. 3B). We also found that reducing the concentration of both polymers in SCFM2, led to the dissolution of stacked aggregates as expected; while it did not affect the formation of PAO1 $\Delta wbpL$ clumped aggregates (Fig. S5). These findings suggests that loss of OSA prevents entropically-derived stacked aggregate assembly, and the associated mechanism is independent of the polymer concentration and/or cell density. This is a well-studied manifestation of aggregation of hydrophobic particles in colloidal environments (44, 45).

Aggregate assembly of *P. aeruginosa* is not serotype specific but dependent on cell surface relative hydrophobicity. There are 20 serotypes of *P. aeruginosa* based on the glycosyl groups of OSA (38). As our findings were limited to PAO1 (serotype O5), we examined the aggregate assembly of PA14 (serotype O10), PAK (serotype O6) and STO1 (serotype O1) which all differ in the oligosaccharide units of OSA (38). We observed a stacked assembly similar to PAO1, but in a STO1 strain lacking OSA ($\Delta wbpM$), we identified small clumped aggregate assembly, with restoration of stacks when *wbpM* was complemented *in trans* (Fig. 4A & B). This data confirms that aggregate assembly type is not serotype specific.

Previously it has been shown that lack of OSA increases the hydrophobicity of the *P. aeruginosa* cell surface (31). We examined whether loss of OSA altered aggregate assembly by changing the cell surface hydrophobicity. We assessed the relative surface hydrophobicity of cells with and without OSA. We

found a significant increase in surface hydrophobicity in strains lacking OSA (Fig. 5A). Loss of OSA is a common adaptive trait of *P. aeruginosa* in CF airways, possibly leading to increase in cell surface hydrophobicity. We therefore evaluated the relative hydrophobicity of 11 *P. aeruginosa* isolates collected from the expectorated sputa of 2 individuals with CF. We observed heterogeneity in cell surface relative hydrophobicity of the CF isolates across the two patients (Fig. 5B).

Discussion

It is now well established that *P. aeruginosa* cells grow within multi-cellular aggregates in expectorated CF sputum (12, 27, 46, 47). Recent studies on the spatial organization of *P. aeruginosa* cells in environments mimicking the chemical and physical properties of CF sputum have demonstrated that aggregates are readily formed in these environments (8, 14, 47). Despite our knowledge of adaptation of *P. aeruginosa* to the CF lung environment (21-23, 33, 48, 49), and population heterogeneity during chronic infection (22, 23, 25, 50), little is known about the impact of this diversity on the organization of *P. aeruginosa* aggregates. To test whether genetic heterogeneity impacts aggregation, we investigated the aggregate formation of selected evolved isolates from a previous 50-day biofilm evolution experiment of PAO1 (25) and examined aggregate formation in SCFM2 (26). We found that (i) there are two distinct types of aggregate assemblies formed by *P. aeruginosa* in SCFM2; (ii) the OSA (B-band) impacts aggregate assembly type and (iii) the loss of OSA and LPS core+1 increases the hydrophobicity of the bacterial surface which prevents depletion aggregation.

Previously it was shown that aggregation of *P. aeruginosa* cells in a polymer rich environment can be due to depletion forces, where minimization of the free energy by increased entropy of the whole system leads to a stacked aggregation of bacterial cells (14). Change of the polymer electrostatic properties in the same study, altered the aggregate assembly to bridging assembly, suggesting that aggregate assembly type is driven by physical properties of the environment, and that the biological properties of the cells assumes little or no role on aggregate assembly type (14). We tested the hypothesis that aggregate formation is also dependent on physiological properties of cells. We observed two distinct types of aggregate assembly by genetically diverse PAO1 isolates in SCFM2; a stacked organized pattern and a clumped disorganized assembly (Fig. 1, Fig. S1). We confirmed that while stacked aggregation is dependent on cell density and polymer concentration (Fig. 3; Fig. S5), and that increase in entropy is the driving force behind these assemblies, the clumping assembly is only driven by changes in surface

properties of *P. aeruginosa* cells (Fig. 2). This finding strongly indicates that although aggregate formation is influenced by physical forces, altering certain bacterial phenotypes can strongly influence the spatial organization enforced by physical properties of the environment.

Other studies have suggested that in CF infections, polymers like mucin can disperse cells in established biofilms (51), although our work suggests that polymers are more likely to influence the spatial arrangement of the cells. The clumping aggregate assembly that we observed was not influenced by factors that have previously been shown to be involved in biofilm and aggregate formation including lectins (42, 52), QS (6, 9, 53) and EPS (47, 54-56) (Fig. S4). It is noteworthy that stacked aggregates form in other species of bacteria such as in *Rhizobium leguminosarum* which was shown to require LPS core and O-antigen to form strong stacked aggregates on roots (57).

In biofilm evolved isolates and clean deletion mutants, we identified that the structure of the O-antigen plays a crucial role in the different aggregate assembly types (Fig. 1 and Fig. 2). In *P. aeruginosa*, LPS contains three major components: the lipid A layer of the outer membrane, a core oligosaccharide and O-antigen components. O-antigens are further subdivided into a D-rhamnose homopolymer found in most strains called the common polysaccharide antigen (CPA or A-band) and a variable heteropolymer of 3 to 5 sugars called the O-specific antigen (OSA or B-band) that confers serotype specificity (31, 32). Specifically, we found that the CPA mutant formed stacked aggregates similar to those seen in a wild-type PAO1, while OSA mutants formed clumping aggregates (Fig. 2). This behavior was independent of the serotype of the *P. aeruginosa* strain suggesting that OSA effects on aggregate formation is not serotype or strain specific (Fig. 4).

The negative charge of *P. aeruginosa* cells in neutral pH, is due to negatively charged phosphoester groups in glycosyl moieties of OSA (32). Previous studies on cation exchange capacity and metal binding domains of PAO1 suggested that in *wbpL* mutants, the total cationic exchange is pH dependent, and most negatively charged moieties are the phosphoesters in the LPS core (58). These suggest that some of the hydrophilic properties of *P. aeruginosa* are due to phosphoesters moieties of the OSA and LPS core. Previous work has shown that LPS composition affects the surface properties of *P. aeruginosa* and loss of both CPA and OSA results in a greater cell surface hydrophobicity (31, 32). By assessing the relative hydrophobicity of cells forming different aggregate types, we found that *P. aeruginosa* cells that

form clumped aggregates have higher relative hydrophobic surfaces. We also found that there is heterogeneity in surface hydrophobicity of *P. aeruginosa* isolates sourced from two CF sputum samples (Fig. 5).

The loss of OSA has been reported in small colony variants of *P. aeruginosa* isolated from CF sputum, suggesting that finding small clumped aggregates in CF sputum might be directly due to the loss of OSA. Regulating aggregate assembly type by directly altering OSA expression levels in environments containing differential levels of cells and polymers (such as CF sputum), may allow cells to better resist environmental stressors such as the host immune response, antibiotics or phage.

Overall, our findings highlight that *P. aeruginosa* cells alter their surface properties which allows them to overcome and adapt to changes in the physicochemical properties of the environment, where loss of OSA allows clumping aggregation even at low cell densities, providing potential benefits from social interactions with highly-related cells. Our findings also highlight that changes in cell surface properties may influence how aggregates form in other species of bacteria and provides explanations as to how different species can stably co-exist in microbiomes.

Materials & Methods

Bacterial strains and culture condition. We selected 7 evolved isolates of PAO1 from 50 day evolved populations in SCFM (25). We transformed all *P. aeruginosa* strains used in this study with pME6032:*gfp* plasmid (59) using electroporation (60). Briefly, to prepare electrocompetent *P. aeruginosa* cells; we grew the bacterial cells in LB broth overnight, we then washed the overnight cultures with 300 mM sucrose solution at room temperature, and then resuspended the bacterial pellets in 1ml of 300 mM sucrose. We then electroporated 50 μ l of electrocompetent cells with 2 μ l of purified plasmid and recovered the cells by addition of 950 μ l of LB broth and incubation at 37 °C/ 200 rpm for 30 mins. We selected the transformed cells by plating out the electroporated bacteria onto LB agar plates supplemented with 300 mg/ml of tetracycline. We obtained the clinical isolates from Emory CF@LANTA Research Center. Patients in this study were aged between 21-29 at the time of collection of the sputum samples. This study was approved by Institutional Review Board (IRB) at Georgia Institute of Technology and Emory University Hospital. A list of all bacterial strains used in this study is available in Table S2.

Determining diversity in colony morphologies. To determine diversity in colony morphology in evolved populations (25), we used a Congo Red based agar media (1% agar, 1xM63 salts (3g monobasic KHPO₄, 7g K₂PO₄, 2g NH₄.2SO₄, pH adjusted to 7.4), 2.5mM magnesium chloride, 0.4 mM calcium chloride, 0.1% casamino acids, 0.1% yeast extracts, 40 mg/L Congo red solution, 100 µM ferrous ammonium sulphate and 0.4% glycerol) (61). We inoculated each evolved isolate in LB broth and incubated for 6 h at 37°C/200 rpm, then we spotted a 10 µl of the culture onto Congo Red agar plates. We incubated the plated at 37°C for 24 h and a further 4 days at room temperature.

Genomic DNA extraction and whole genome sequencing. We plated each of the selected evolved isolates on LB agar plates, picked single colonies of each isolate and then inoculated in 5 ml of SCFM (35) and incubated overnight at 37 °C/ 200 rpm. We extracted the genomic DNA using the QIAGEN Blood and Tissue DNAeasy kit. We prepared sequencing libraries using the NexteraXT protocol (Illumina), and sequenced in 24-plex on the Illumina MiSeq platform to obtain an approximate calculated level of coverage of 50× for each evolved isolate. For SNP calling, we used breseq analysis (consensus mode) (37, 62, 63) and compared the genetic variation in each evolved isolate to the PAO1 ancestral strain. The sequences are available at the NCBI SRA database (PRJNA702741).

Image acquisition and analysis. For imaging aggregates in SCFM2 (26), we inoculated each bacterial isolate into TSB-broth supplemented with 300 µg/ml of tetracycline and incubated at 37 °C/200 rpm overnight. We inoculated 50 µl of the overnight culture into 5 ml of SCFM and incubated at 37 °C/ 200 rpm for 5-6 hours, until cultures reached mid-log phase (OD₆₀₀ @ 0.5). We then adjusted the OD₆₀₀ to 0.05 in 400 µl of freshly made SCFM2 containing 0.6 mg/ml of DNA and 5 mg/ml of mucin (8, 26). We incubated the cultures at 37 °C for 16 h in chamber slides (Lab-Tek®) before image acquisition. We used a confocal LSM880 microscope equipped with a 63× oil immersion lens for image acquisition and scanned the aggregates using diode laser 488 nm, and collected fluorescent emission between 480-530 nm for image acquisition. For imaging the cells grown in SCFM, we adjusted the OD₆₀₀ of cells from mid-log phase growth to 0.05 in 400 µl of freshly made SCFM. We incubated the cultures at 37 °C for 16 h in chamber slides before image acquisition. For image analysis, we used Imaris 9.0.1 image analysis software to analyze the morphological properties of the aggregates and measured the surface area and volume of each aggregate using a surface model algorithm. We measured the aggregate volume and

surface area in 10 images acquired for each strain in three independent experiments (over 1000 aggregates were measured in total for each condition). For time course experiments, we used the same image acquisition parameters, using the time series option and imaged as Z stacks every 20 minutes for up to 10 hours. To assess the role of bacterial cell density on aggregation, we adjusted the OD₆₀₀ to 0.1 in 400 µl of SCFM2 and imaged the cells every 20 minutes for 6 hours. We prepared time series videos using the 3D plugin in Fiji (64) and Adobe Lightroom.

Gene deletion and complementation. We used standard genetic techniques for the construction of *P. aeruginosa* mutants. To delete *ssg*, *rmd*, *wbpL*, *wbpM*, *waaL*, *wzy*, *wzz1* and *wzz2*, we PCR amplified 600 bp DNA sequences flanking the open reading frame of each gene using Q5 DNA polymerase (New England Biolabs). We then cloned these sequences into EcoRI-XbaI digested pEXG2 by Gibson assembly using NEBuilder HiFi Assembly master mix (New England Biolabs) and transformed into *E.coli* S17 λpir. We verified cloned inserts by colony PCR and Sanger sequencing (Eurofins Genomics). We introduced the deletion constructs into PAO1 by electroporation and selected strains carrying single crossover insertions of the deletion constructs on LB agar plates supplemented with 100 µg/mL gentamycin. We cultured gentamycin resistant colonies in LB without antibiotic and plated on LB agar plates with 0.25% NaCl and 5% sucrose. We then selected sucrose resistant colonies and screened them for gentamycin sensitivity to ensure loss of the pEXG2 construct and assessed them for the desired gene deletion by colony PCR and Sanger sequencing of the PCR product. For *ssg* complementation we PCR amplified the *ssg* coding sequence and 100 bp upstream sequence (including the *ssg* native promoter) using Q5 DNA polymerase (New England Biolabs). We cloned this 1057 bp product into KpnI-BamHI digested pUC18T-miniTn7-Gent by Gibson assembly using NEBuilder HiFi Assembly master mix (New England Biolabs) and transformed into *E.coli* S17 λpir. We verified the cloned insert by colony PCR and Sanger sequencing (Eurofins Genomics). We co-transformed the complementation construct with the Tn7 helper plasmid pTNS3 into PAO1Δ*ssg* and evolved isolates by electroporation and selected on LB agar plates supplemented with 100 µg/mL gentamycin. We verified the strains for *ssg*⁺ complementation by colony PCR and for loss of pUC18-miniTn7-Gent vector and pTNS3 by screening for carbenicillin sensitivity.

LPS extraction. We isolated bacterial lipopolysaccharide by the hot phenol extraction method (65). Briefly, we pelleted 5 mL overnight cultures of PAO1 and PAO1-derived strains in LB broth by

centrifugation for 10 min at 4200×g. We resuspended the pellets in 200 µL 1X SDS buffer (2% β-mercaptoethanol (BME), 2% SDS, 10% glycerol, 50 mM Tris-HCl, pH 6.8) and incubated at 99°C for 15 min. Then we added 5 µL of 20 mg/mL proteinase K (Sigma) to each tube and incubated cell lysates at 59°C for 3 hours. Then we added 200 µl of ice-cold Tris-saturated phenol to each sample, vortexed for 10 min, then added 1 mL diethyl-ether and vortexed for a further 10 seconds. We centrifuged the samples for 10 min at 16000Xg and extracted the bottom layer. We performed a second extraction with phenol and diethyl-ether as above. We mixed an equal volume of the extracted LPS samples with an equal volume of 2X SDS buffer and electrophoresed 10 µL of each sample on Novex 4-20% polyacrylamide gradient gels (ThermoFisher) in Tris-Glycine-SDS buffer. Following electrophoresis, we visualized LPS with a ProQ Emerald Lipopolysaccharide staining kit (ThermoFisher).

Assessing cell surface hydrophobicity. To assess the levels of cell surface hydrophobicity, we used hydrophobic interaction chromatography (31). Briefly, we grew bacterial cells for 6-8 h at 37 °C/ 200 rpm, to reach mid-log phase. We harvested the cells and washed the cells 3× with ice cold 3M NaCl pH=7 and resuspended in 3M NaCl. We used octyl-Sepharose CL-4C beads (SIGMA) to assess the interaction of hydrophobic cells to these beads compared to control Sepharose CL-4C beads (SIGMA). We prepared bead columns by a 3× wash of the beads with Mili-Q water, and then 3× washes with 3M NaCl (pH=7) (at 4°C). We then prepared 1 ml columns of both beads by using 3 ml diameter filter paper. We added 100 µl of bacterial suspension and incubated at room temperature for 15 minutes. We measured the OD₄₅₀ of flow through from each column. We calculated the relative hydrophobicity based on the ratio of OD₄₅₀ octyl-Sepharose CL-C4 column flow through and control column.

Statistical analysis. For statistical analysis of the aggregate volume and biovolume distribution, we used GraphPad Prism 8.0.

Figure legends

Fig. 1. The two types of aggregate assembly formed by *P. aeruginosa* isolates in SCFM2 is due to *ssg* gene mutation. (A) In PAO1 and evolved isolates, aggregates assembled into either organized stacked structures (labeled as S) or disorganized clumps (labeled as C). (B) Stacked aggregates of PAO1 and A2 were significantly larger than aggregates formed by A9 and B9, and complementation with an

intact *ssg* gene significantly increased the aggregate volume (Kruskal-Wallis, Dunn's multiple comparison test, $p < 0.0001$; error bars are median with interquartile range of aggregate volume, each data point is representative of an aggregate).

Fig. 2. Loss of OSA leads to clumped aggregate assembly. (A) Loss of CPA (Δrmd) did not alter the type of aggregate assembly, and loss of OSA ($\Delta wbpM$) lead to dispersed small aggregates. The loss of both CPA and OSA ($\Delta wbpL$) changed aggregate assembly type similar to the *ssg* mutant. (B) There was a significant reduction in aggregate volume in *ssg*, *wbpL* and *wbpM* mutants, however only the loss of *ssg* and *wbpL* displayed large clumped aggregates (Kruskal-Wallis, Dunn's multiple comparison test, $p < 0.0001$; error bars are median with interquartile range of aggregate volume, each point is representative of an aggregate).

Fig. 3. Clumped aggregate assembly is not dependent on cell density. (A) The aggregate biovolume of PAO1 significantly increase after 180 minutes of growth (median biovolume = 0.34-0.75 over time). (B) In PAO1 $\Delta wbpL$ (lacking OSA), biovolume remained the same over time (median biovolume = 0.33-0.27 over time).

Fig. 4. Clumped Aggregate assembly of *P. aeruginosa* is not serotype specific. (A) *P. aeruginosa* PA14 and PAK and STO1 formed stacked aggregates in SCFM2 and loss of OSA in STO1(STO1 $\Delta wbpM$) lead to clumped assembly of aggregates. (B) Loss of OSA altered aggregate assembly from stacked to clumped in STO1 and significantly decreased aggregate volume (Kruskal-Wallis, Dunn's multiple comparison test, $p = 0.0048$; error bars are median with interquartile range of aggregate volume, each data point is representative of an aggregate).

Fig. 5. Cell surface hydrophobicity determines the aggregate assembly type. (A) The relative cell surface hydrophobicity was dependent on OSA, and mutation in *ssg*, *wbpL* and *wbpM* lead to an increase in relative hydrophobicity in PAO1 and STO1 (Green bars). (B) There was heterogeneity in the relative hydrophobicity of cell surfaces in *P. aeruginosa* isolates collected from two CF expectorated sputum samples (CFP1 and CFP2).

Supplemental figure legends

Fig. S1. Aggregate assembly of PAO1 evolved isolates in SCFM2. (A) Evolved isolates of PAO1 displayed differential colony morphologies on Congo red agar plates. (B) Evolved isolates B8, B13, C25 and D4 displayed stacked aggregate assembly (labeled as S). (C) There were no significant differences in the volume of stacked aggregates in these isolates compared to PAO1 ($p < 0.0001$, Kruskal-Wallis, Dunn's multiple comparison test, error bars are median with interquartile range of aggregate volume).

Fig. S2. Mutation in PA5001 (*ssg*) in PAO1 switches the stacked aggregate assembly to clumped assembly. (A) PAO1 and A2 cells formed a dispersed layer of cells on cover slips when grown in SCFM (without any polymer), while A9 and B9 formed small clumps in SCFM. (B) Complementing A9 and B9 isolates with *ssg* restored the aggregate assembly to stacked (Kruskal-Wallis, Dunn's multiple comparison test, $p < 0.0001$, error bars are median with interquartile range of aggregate volume).

Fig. S3. Loss of *ssg* function changes the LPS OSA profile in *P. aeruginosa*. (A) Evolved isolates of PAO1 with 1 bp deletion in *ssg* had the same OSA profile as PAO1 Δ_{ssg} , and complementation of *ssg* in *trans* restored the OSA pattern. (B) Loss of *ssg* resulted in the loss of OSA and a change in capped core pattern.

Fig. S4. The aggregate assembly type is independent of exopolysaccharide production, lectins and quorum sensing. (A) Loss of lectins (Δ_{lecA} and Δ_{lecB}), quorum sensing (Δ_{lasR}) and exopolysaccharide components ($\Delta_{pel/psl}$) did not change the aggregate assembly type and aggregates were assembled in stacked form similar to those seen in PAO1. (B) Stacked aggregates formed by cells lacking lectins (Δ_{lecA} and Δ_{lecB}), quorum sensing (Δ_{lasR}) and exopolysaccharide components ($\Delta_{pel/psl}$) were the same size as PAO1 aggregates.

Fig. S5. Stacked aggregate assembly is dependent on the concentration of both eDNA and mucin. (A) Stacked aggregate formation was disrupted by diluting polymers in SCFM2. (B) Clumped aggregate assembly was independent of the polymer concentration in the environment.

Movie S1. Increased cell density reduced the time of stacked aggregation. To determine whether stacked aggregate assembly was dependent on cell density, we monitored the growth of PAO1 over time

(initial density adjusted OD₆₀₀ to 0.1 in 400 µl of SCFM2). Stacked aggregates were assembled after 180 minutes of growth.

Movie S2. Increased cell density does not impact the timing of formation of clumped aggregation.

We monitored the growth of PAO1Δ*wbpL* (initial density adjusted OD₆₀₀ to 0.1 in 400 µl of SCFM2). There was no change in aggregate assembly over time.

Dataset 1. List of SNPs in 7 evolved isolates of PAO1.

Table S1. Stacked aggregates have higher biovolume than clumped aggregates. To determine the differences in biomass of each aggregate type, we calculated the total biovolume of all aggregates in each acquired image, using Imaris. There was a significant difference between distribution of biovolume of stacked and clumped (green) aggregates (Kruskal-Wallis, Dunn's multiple comparison test, $p < 0.0001$; error bars are median with interquartile range of aggregate biovolume).

Table S2. List of the strains used in this study.

Acknowledgments. For funding, we thank the Georgia Institute of Technology; The Cystic Fibrosis Foundation for grants (DIGGLE18I0; DIGGLE20G0) to SPD and a Fellowship to SA (AZIMI18F0); CF@latna for a Fellowship to SA (3206AXB); The National Institute for Health (R56AI153116) to SPD; the National Science Foundation (1806606) to JEC. We thank Marvin Whiteley for useful discussion and use of his Confocal Zeiss LSM880 and Imaris image analysis platform. Access to the CF Biospecimen Registry (CFBR) at Emory Children's Center for Cystic Fibrosis and Airways Disease Research was provided through Children's Healthcare of Atlanta and the Emory University Pediatric CF Discovery Core. We thank Arlene Stecenko and Katie Clemmer for assistance acquiring bacterial isolates.

Conflict of interest statement. The authors declare no conflict of interest with any of the work presented in this manuscript.

References

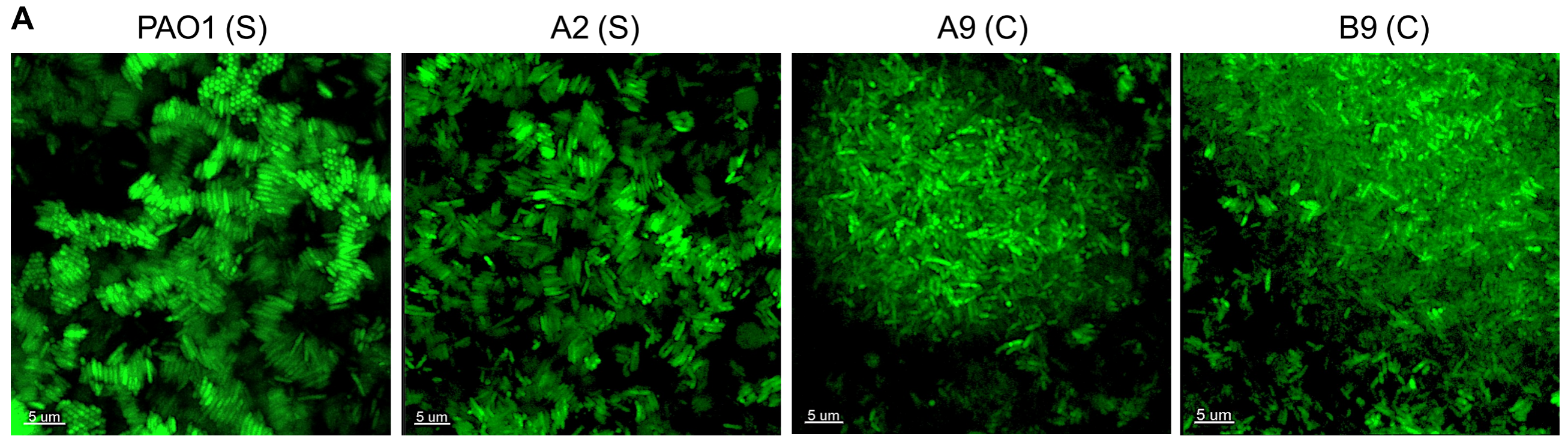
1. Kragh KN, Alhede M, Jensen PO, Moser C, Scheike T, Jacobsen CS, Seier Poulsen S, Eickhardt-Sorensen SR, Trostrup H, Christoffersen L, Hougen HP, Rickelt LF, Kuhl M, Hoiby N, Bjarnsholt T. 2014. Polymorphonuclear leukocytes restrict growth of *Pseudomonas aeruginosa* in the lungs of cystic fibrosis patients. *Infect Immun* 82:4477-86.
2. Hall CW, Mah TF. 2017. Molecular mechanisms of biofilm-based antibiotic resistance and tolerance in pathogenic bacteria. *FEMS Microbiol Rev* 41:276-301.
3. Pang Z, Raudonis R, Glick BR, Lin TJ, Cheng Z. 2019. Antibiotic resistance in *Pseudomonas aeruginosa*: mechanisms and alternative therapeutic strategies. *Biotechnol Adv* 37:177-192.
4. West SA, Griffin AS, Gardner A, Diggle SP. 2006. Social evolution theory for microorganisms. *Nat Rev Microbiol* 4:597-607.
5. Xavier JB, Foster KR. 2007. Cooperation and conflict in microbial biofilms. *Proc Natl Acad Sci U S A* 104:876-81.
6. Whiteley M, Diggle SP, Greenberg EP. 2017. Progress in and promise of bacterial quorum sensing research. *Nature* 551:313-320.
7. Popat R, Crusz SA, Messina M, Williams P, West SA, Diggle SP. 2012. Quorum-sensing and cheating in bacterial biofilms. *Proc Biol Sci* 279:4765-71.
8. Darch SE, Simoska O, Fitzpatrick M, Barraza JP, Stevenson KJ, Bonnacaze RT, Shear JB, Whiteley M. 2018. Spatial determinants of quorum signaling in a *Pseudomonas aeruginosa* infection model. *Proc Natl Acad Sci U S A* 115:4779-4784.
9. Azimi S, Klementiev AD, Whiteley M, Diggle SP. 2020. Bacterial Quorum Sensing During Infection. *Annu Rev Microbiol* 74:201-219.
10. Bjarnsholt T, Alhede M, Alhede M, Eickhardt-Sorensen SR, Moser C, Kuhl M, Jensen PO, Hoiby N. 2013. The in vivo biofilm. *Trends Microbiol* 21:466-74.
11. Roberts AE, Kragh KN, Bjarnsholt T, Diggle SP. 2015. The Limitations of In Vitro Experimentation in Understanding Biofilms and Chronic Infection. *J Mol Biol* 427:3646-61.
12. Kragh KN, Hutchison JB, Melaugh G, Rodesney C, Roberts AE, Irie Y, Jensen PO, Diggle SP, Allen RJ, Gordon V, Bjarnsholt T. 2016. Role of Multicellular Aggregates in Biofilm Formation. *mBio* 7:e00237.
13. Darch SE, Kragh KN, Abbott EA, Bjarnsholt T, Bull JJ, Whiteley M. 2017. Phage Inhibit Pathogen Dissemination by Targeting Bacterial Migrants in a Chronic Infection Model. *MBio* 8.
14. Secor PR, Michaels LA, Ratjen A, Jennings LK, Singh PK. 2018. Entropically driven aggregation of bacteria by host polymers promotes antibiotic tolerance in *Pseudomonas aeruginosa*. *Proc Natl Acad Sci U S A* 115:10780-10785.
15. Liu HH, Yang YR, Shen XC, Zhang ZL, Shen P, Xie ZX. 2008. Role of DNA in bacterial aggregation. *Curr Microbiol* 57:139-44.
16. Dorken G, Ferguson GP, French CE, Poon WC. 2012. Aggregation by depletion attraction in cultures of bacteria producing exopolysaccharide. *J R Soc Interface* 9:3490-502.
17. Harris RH, Mitchell R. 1973. The role of polymers in microbial aggregation. *Annu Rev Microbiol* 27:27-50.
18. Strand SP, Nordengen T, Ostgaard K. 2002. Efficiency of chitosans applied for flocculation of different bacteria. *Water Res* 36:4745-52.
19. Schweizer JBHaKS. 2005. Contact Aggregation, Bridging, and Steric Stabilization in Dense Polymer-Particle Mixtures. *Macromolecules* 38:8858-8869.

20. Das T, Sharma PK, Busscher HJ, van der Mei HC, Krom BP. 2010. Role of extracellular DNA in initial bacterial adhesion and surface aggregation. *Appl Environ Microbiol* 76:3405-8.
21. Marvig RL, Sommer LM, Molin S, Johansen HK. 2015. Convergent evolution and adaptation of *Pseudomonas aeruginosa* within patients with cystic fibrosis. *Nat Genet* 47:57-64.
22. Darch SE, McNally A, Harrison F, Corander J, Barr HL, Paszkiewicz K, Holden S, Fogarty A, Crusz SA, Diggle SP. 2015. Recombination is a key driver of genomic and phenotypic diversity in a *Pseudomonas aeruginosa* population during cystic fibrosis infection. *Sci Rep* 5:7649.
23. Williams D, Evans B, Haldenby S, Walshaw MJ, Brockhurst MA, Winstanley C, Paterson S. 2015. Divergent, coexisting *Pseudomonas aeruginosa* lineages in chronic cystic fibrosis lung infections. *Am J Respir Crit Care Med* 191:775-85.
24. Rossi E, La Rosa R, Bartell JA, Marvig RL, Haagensen JAJ, Sommer LM, Molin S, Johansen HK. 2020. *Pseudomonas aeruginosa* adaptation and evolution in patients with cystic fibrosis. *Nat Rev Microbiol* doi:10.1038/s41579-020-00477-5.
25. Azimi S, Roberts AEL, Peng S, Weitz JS, McNally A, Brown SP, Diggle SP. 2020. Allelic polymorphism shapes community function in evolving *Pseudomonas aeruginosa* populations. *ISME J* doi:10.1038/s41396-020-0652-0.
26. Turner KH, Wessel AK, Palmer GC, Murray JL, Whiteley M. 2015. Essential genome of *Pseudomonas aeruginosa* in cystic fibrosis sputum. *Proc Natl Acad Sci U S A* 112:4110-5.
27. DePas WH, Starwalt-Lee R, Van Sambeek L, Ravindra Kumar S, Gradinaru V, Newman DK. 2016. Exposing the Three-Dimensional Biogeography and Metabolic States of Pathogens in Cystic Fibrosis Sputum via Hydrogel Embedding, Clearing, and rRNA Labeling. *mBio* 7.
28. Veeranagouda Y, Lee K, Cho AR, Cho K, Anderson EM, Lam JS. 2011. Ssg, a putative glycosyltransferase, functions in lipo- and exopolysaccharide biosynthesis and cell surface-related properties in *Pseudomonas alkylphenolia*. *FEMS Microbiol Lett* 315:38-45.
29. Fernandez L, Alvarez-Ortega C, Wiegand I, Olivares J, Kocincova D, Lam JS, Martinez JL, Hancock RE. 2013. Characterization of the polymyxin B resistome of *Pseudomonas aeruginosa*. *Antimicrob Agents Chemother* 57:110-9.
30. Pan X, Cui X, Zhang F, He Y, Li L, Yang H. 2016. Genetic Evidence for O-Specific Antigen as Receptor of *Pseudomonas aeruginosa* Phage K8 and Its Genomic Analysis. *Front Microbiol* 7:252.
31. Makin SA, Beveridge TJ. 1996. The influence of A-band and B-band lipopolysaccharide on the surface characteristics and adhesin of *Pseudomonas aeruginosa* to surfaces. *Microbiology* 142:299-307.
32. Rocchetta HL, Burrows LL, Lam JS. 1999. Genetics of O-antigen biosynthesis in *Pseudomonas aeruginosa*. *Microbiol Mol Biol Rev* 63:523-53.
33. Marvig RL, Dolce D, Sommer LM, Petersen B, Ciofu O, Campana S, Molin S, Taccetti G, Johansen HK. 2015. Within-host microevolution of *Pseudomonas aeruginosa* in Italian cystic fibrosis patients. *BMC Microbiol* 15:218.
34. Jorth P, Staudinger BJ, Wu X, Hisert KB, Hayden H, Garudathri J, Harding CL, Radey MC, Rezayat A, Bautista G, Berrington WR, Goddard AF, Zheng C, Angermeyer A, Brittnacher MJ, Kitzman J, Shendure J, Fligner CL, Mittler J, Aitken ML, Manoil C, Bruce JE, Yahr TL, Singh PK. 2015. Regional Isolation Drives Bacterial Diversification within Cystic Fibrosis Lungs. *Cell Host Microbe* 18:307-19.
35. Palmer KL, Mashburn LM, Singh PK, Whiteley M. 2005. Cystic fibrosis sputum supports growth and cues key aspects of *Pseudomonas aeruginosa* physiology. *J Bacteriol* 187:5267-77.
36. Palmer KL, Aye LM, Whiteley M. 2007. Nutritional cues control *Pseudomonas aeruginosa* multicellular behavior in cystic fibrosis sputum. *J Bacteriol* 189:8079-87.

37. Barrick JE, Colburn G, Deatherage DE, Traverse CC, Strand MD, Borges JJ, Knoester DB, Reba A, Meyer AG. 2014. Identifying structural variation in haploid microbial genomes from short-read resequencing data using breseq. *BMC Genomics* 15:1039.
38. Huszczyński SM, Lam JS, Khursigara CM. 2019. The Role of *Pseudomonas aeruginosa* Lipopolysaccharide in Bacterial Pathogenesis and Physiology. *Pathogens* 9.
39. Li Y, Xia H, Bai F, Song X, Zhuang L, Xu H, Zhang X, Zhang X, Qiao M. 2020. PA5001 gene involves in swimming motility and biofilm formation in *Pseudomonas aeruginosa*. *Microb Pathog* 144:103982.
40. Kintz E, Goldberg JB. 2008. Regulation of lipopolysaccharide O antigen expression in *Pseudomonas aeruginosa*. *Future Microbiol* 3:191-203.
41. Cross AR, Goldberg JB. 2019. Remodeling of O Antigen in Mucoid *Pseudomonas aeruginosa* via Transcriptional Repression of *wzz2*. *mBio* 10.
42. Diggle SP, Stacey RE, Dodd C, Camara M, Williams P, Winzer K. 2006. The galactophilic lectin, LecA, contributes to biofilm development in *Pseudomonas aeruginosa*. *Environ Microbiol* 8:1095-104.
43. Colvin KM, Gordon VD, Murakami K, Borlee BR, Wozniak DJ, Wong GC, Parsek MR. 2011. The *pel* polysaccharide can serve a structural and protective role in the biofilm matrix of *Pseudomonas aeruginosa*. *PLoS Pathog* 7:e1001264.
44. Lopez-Leon T, Ortega-Vinuesa JL, Bastos-Gonzalez D. 2012. Ion-specific aggregation of hydrophobic particles. *Chemphyschem* 13:2382-91.
45. Sanchez-Iglesias A, Grzelczak M, Altantzis T, Goris B, Perez-Juste J, Bals S, Van Tendeloo G, Donaldson SH, Jr., Chmelka BF, Israelachvili JN, Liz-Marzan LM. 2012. Hydrophobic interactions modulate self-assembly of nanoparticles. *ACS Nano* 6:11059-65.
46. Sonderholm M, Kragh KN, Koren K, Jakobsen TH, Darch SE, Alhede M, Jensen PO, Whiteley M, Kuhl M, Bjarnsholt T. 2017. *Pseudomonas aeruginosa* Aggregate Formation in an Alginate Bead Model System Exhibits In Vivo-Like Characteristics. *Appl Environ Microbiol* 83.
47. Jennings LK, Dreifus JE, Reichhardt C, Storek KM, Secor PR, Wozniak DJ, Hisert KB, Parsek MR. 2021. *Pseudomonas aeruginosa* aggregates in cystic fibrosis sputum produce exopolysaccharides that likely impede current therapies. *Cell Rep* 34:108782.
48. Marvig RL, Damkiaer S, Khademi SM, Markussen TM, Molin S, Jelsbak L. 2014. Within-host evolution of *Pseudomonas aeruginosa* reveals adaptation toward iron acquisition from hemoglobin. *mBio* 5:e00966-14.
49. Smith EE, Buckley DG, Wu Z, Saenphimmachak C, Hoffman LR, D'Argenio DA, Miller SI, Ramsey BW, Speert DP, Moskowitz SM, Burns JL, Kaul R, Olson MV. 2006. Genetic adaptation by *Pseudomonas aeruginosa* to the airways of cystic fibrosis patients. *Proc Natl Acad Sci U S A* 103:8487-92.
50. Workentine ML, Sibley CD, Glezerson B, Purighalla S, Norgaard-Gron JC, Parkins MD, Rabin HR, Surette MG. 2013. Phenotypic heterogeneity of *Pseudomonas aeruginosa* populations in a cystic fibrosis patient. *PLoS One* 8:e60225.
51. Co JY, Carcamo-Oyarce G, Billings N, Wheeler KM, Grindy SC, Holten-Andersen N, Ribbeck K. 2018. Mucins trigger dispersal of *Pseudomonas aeruginosa* biofilms. *NPJ Biofilms Microbiomes* 4:23.
52. Passos da Silva D, Matwichuk ML, Townsend DO, Reichhardt C, Lamba D, Wozniak DJ, Parsek MR. 2019. The *Pseudomonas aeruginosa* lectin LecB binds to the exopolysaccharide Psl and stabilizes the biofilm matrix. *Nat Commun* 10:2183.

53. Davies DG, Parsek MR, Pearson JP, Iglewski BH, Costerton JW, Greenberg EP. 1998. The involvement of cell-to-cell signals in the development of a bacterial biofilm. *Science* 280:295-8.
54. Ma L, Wang S, Wang D, Parsek MR, Wozniak DJ. 2012. The roles of biofilm matrix polysaccharide Psl in mucoid *Pseudomonas aeruginosa* biofilms. *FEMS Immunol Med Microbiol* 65:377-80.
55. Jennings LK, Storek KM, Ledvina HE, Coulon C, Marmont LS, Sadovskaya I, Secor PR, Tseng BS, Scian M, Filloux A, Wozniak DJ, Howell PL, Parsek MR. 2015. Pel is a cationic exopolysaccharide that cross-links extracellular DNA in the *Pseudomonas aeruginosa* biofilm matrix. *Proc Natl Acad Sci U S A* 112:11353-8.
56. Irie Y, Roberts AEL, Kragh KN, Gordon VD, Hutchison J, Allen RJ, Melaugh G, Bjarnsholt T, West SA, Diggle SP. 2017. The *Pseudomonas aeruginosa* PSL Polysaccharide Is a Social but Noncheatable Trait in Biofilms. *mBio* 8.
57. Russo DM, Abdian PL, Posadas DM, Williams A, Voza N, Giordano W, Kannenberg E, Downie JA, Zorreguieta A. 2015. Lipopolysaccharide O-chain core region required for cellular cohesion and compaction of in vitro and root biofilms developed by *Rhizobium leguminosarum*. *Appl Environ Microbiol* 81:1013-23.
58. Shephard J, McQuillan AJ, Bremer PJ. 2008. Mechanisms of Cation Exchange by *Pseudomonas aeruginosa* PAO1 and PAO1 wbpL, a Strain with a Truncated Lipopolysaccharide. *Appl Environ Microbiol* 74:6980-6.
59. Heeb S, Itoh Y, Nishijyo T, Schnider U, Keel C, Wade J, Walsh U, O'Gara F, Haas D. 2000. Small, stable shuttle vectors based on the minimal pVS1 replicon for use in gram-negative, plant-associated bacteria. *Mol Plant Microbe Interact* 13:232-7.
60. Smith AW, Iglewski BH. 1989. Transformation of *Pseudomonas aeruginosa* by electroporation. *Nucleic Acids Res* 17:10509.
61. Mayer-Hamblett N, Rosenfeld M, Gibson RL, Ramsey BW, Kulasekara HD, Retsch-Bogart GZ, Morgan W, Wolter DJ, Pope CE, Houston LS, Kulasekara BR, Khan U, Burns JL, Miller SI, Hoffman LR. 2014. *Pseudomonas aeruginosa* in vitro phenotypes distinguish cystic fibrosis infection stages and outcomes. *Am J Respir Crit Care Med* 190:289-97.
62. Barrick JE, Lenski RE. 2013. Genome dynamics during experimental evolution. *Nat Rev Genet* 14:827-39.
63. Deatherage DE, Traverse CC, Wolf LN, Barrick JE. 2014. Detecting rare structural variation in evolving microbial populations from new sequence junctions using breseq. *Front Genet* 5:468.
64. Schindelin J, Arganda-Carreras I, Frise E, Kaynig V, Longair M, Pietzsch T, Preibisch S, Rueden C, Saalfeld S, Schmid B, Tinevez JY, White DJ, Hartenstein V, Eliceiri K, Tomancak P, Cardona A. 2012. Fiji: an open-source platform for biological-image analysis. *Nat Methods* 9:676-82.
65. Davis MR, Jr., Muszynski A, Lollett IV, Pritchett CL, Carlson RW, Goldberg JB. 2013. Identification of the mutation responsible for the temperature-sensitive lipopolysaccharide O-antigen defect in the *Pseudomonas aeruginosa* cystic fibrosis isolate 2192. *J Bacteriol* 195:1504-14.

Figure 1



B

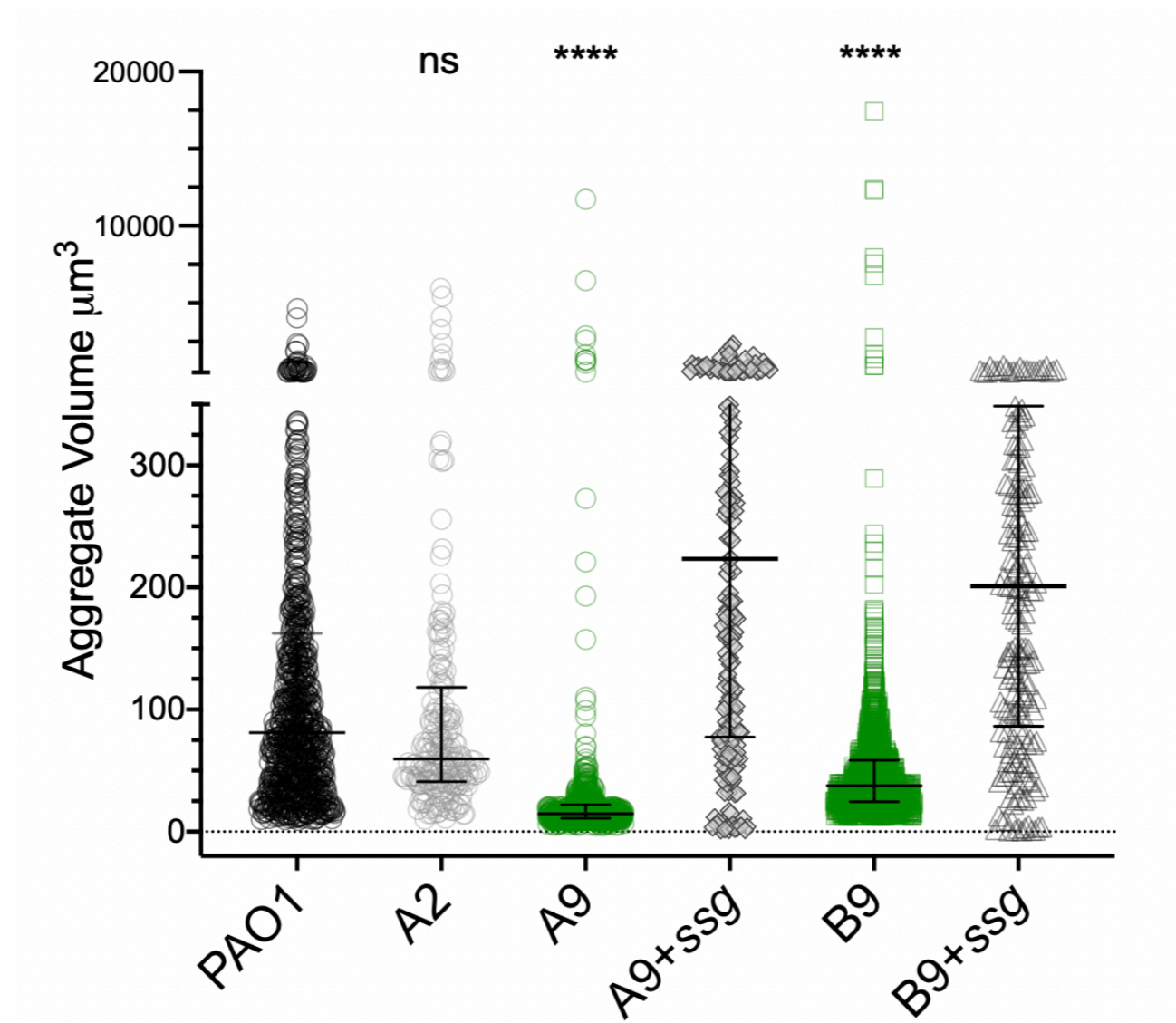


Figure 2

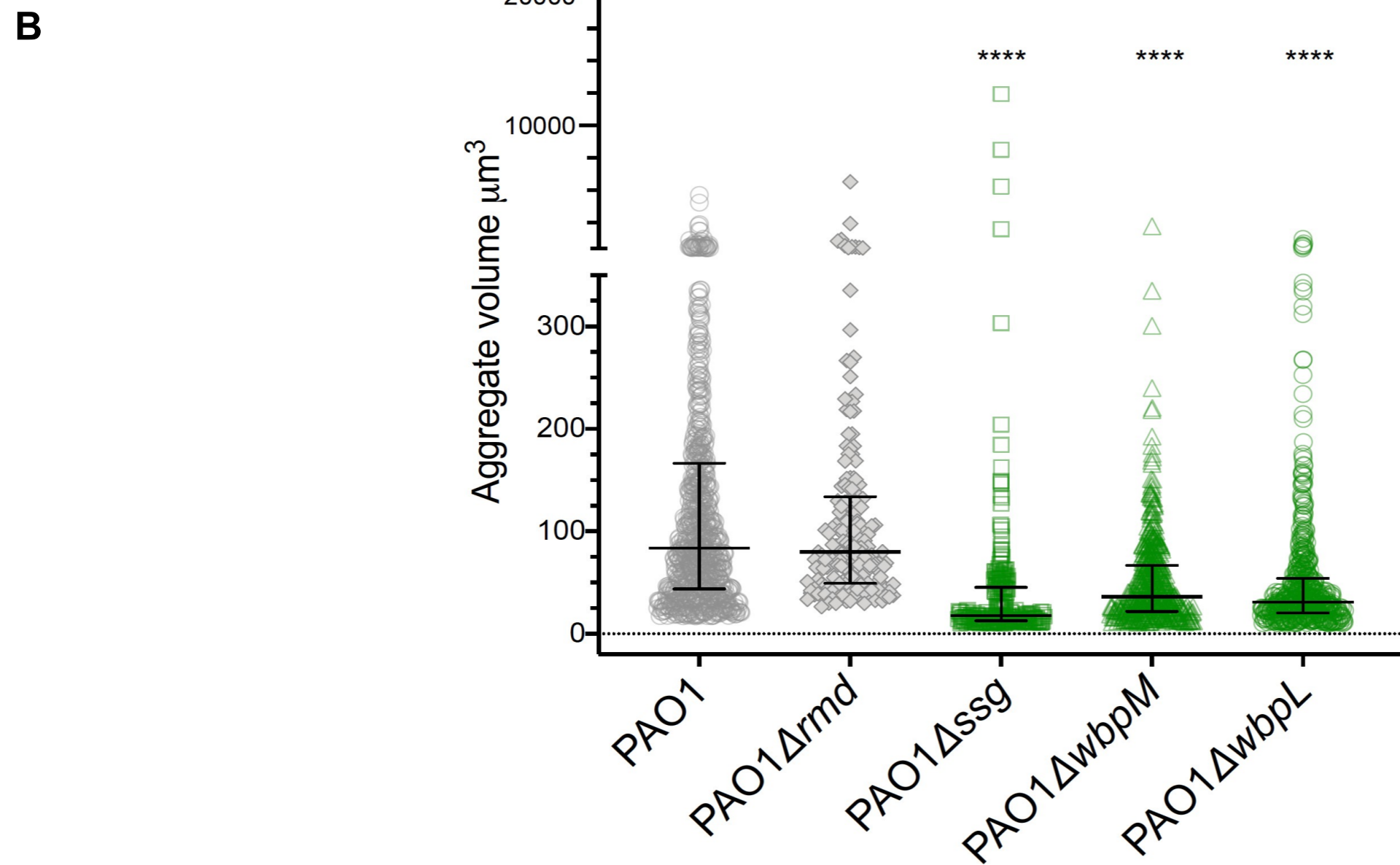
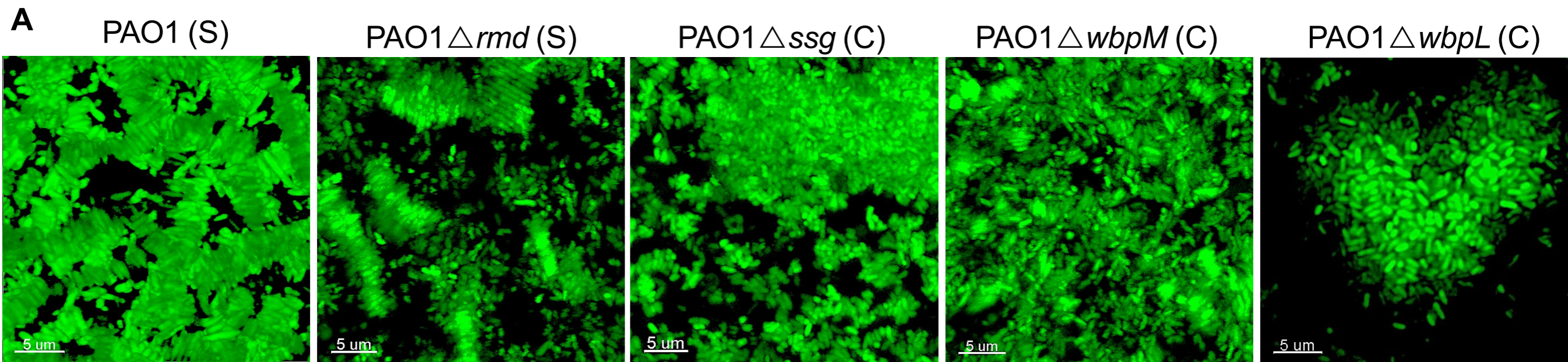


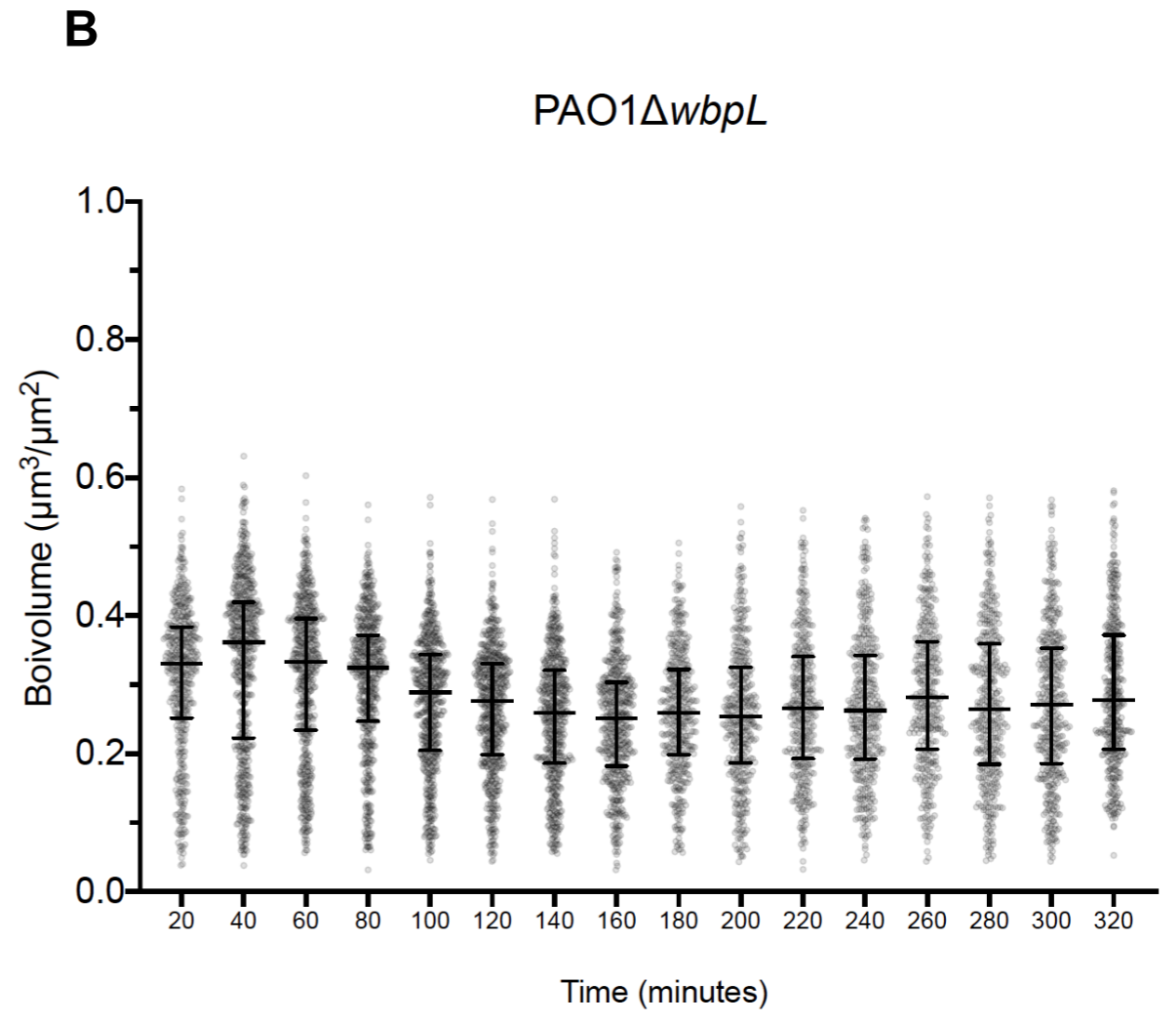
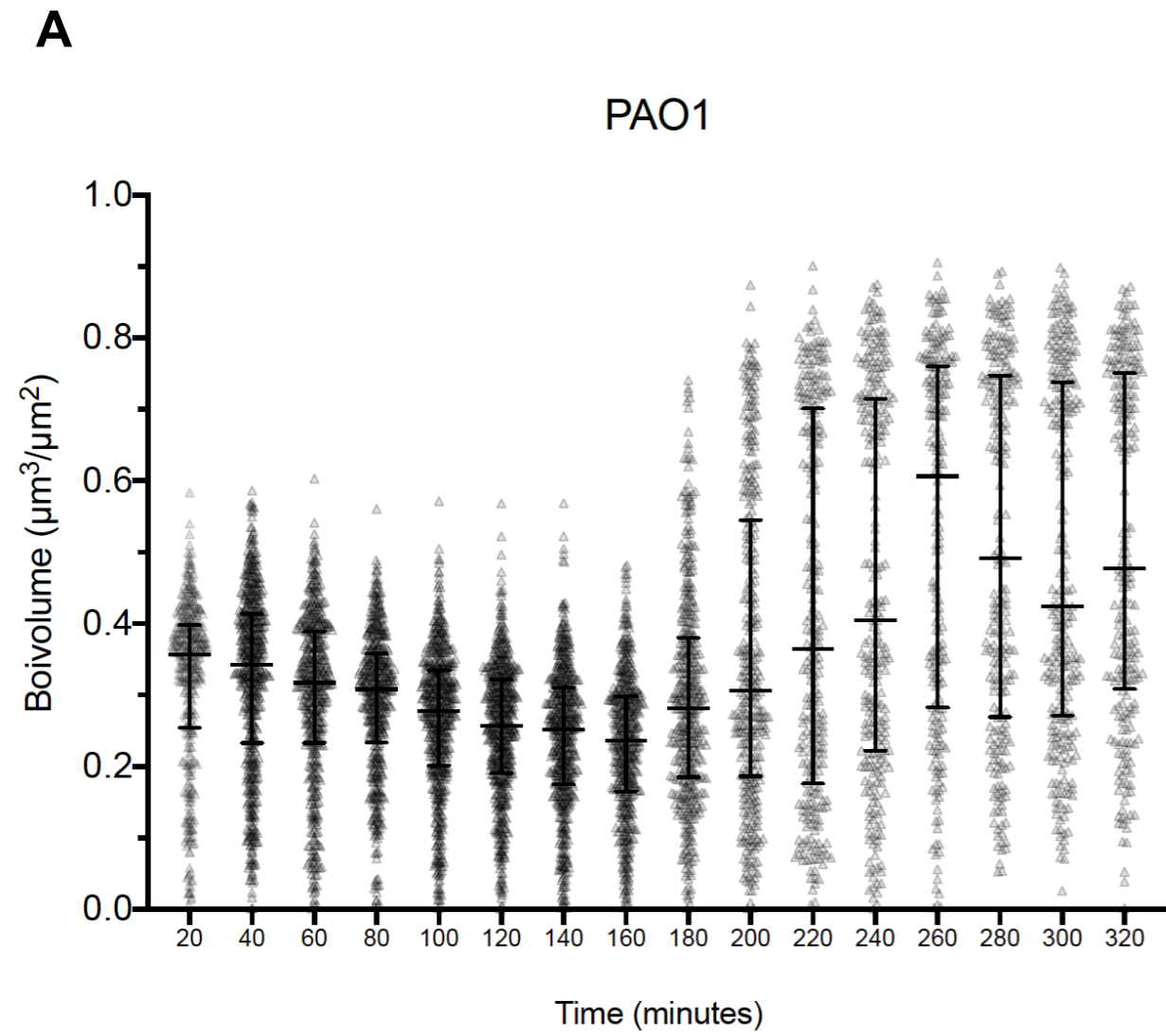
Figure 3

Figure 4

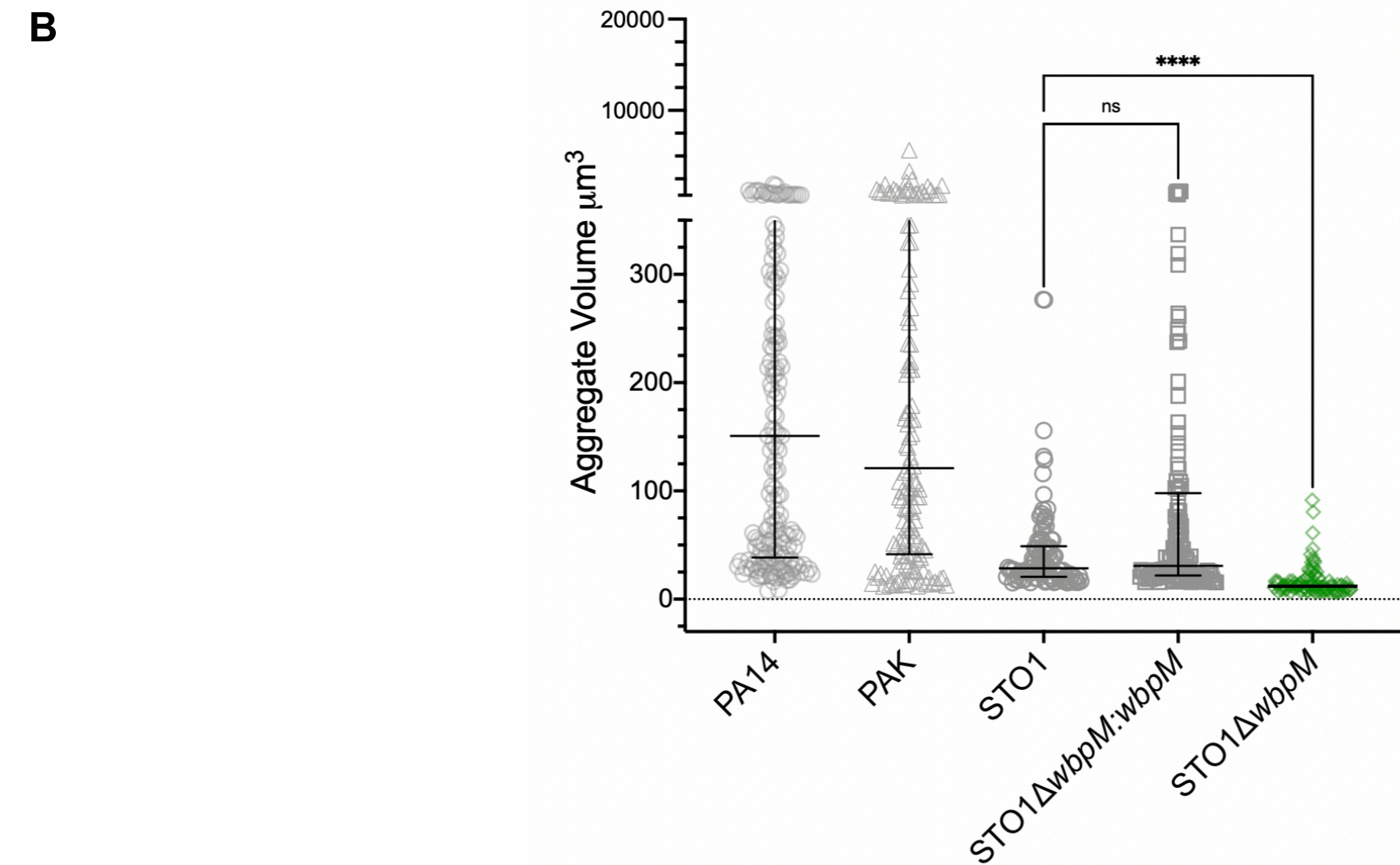
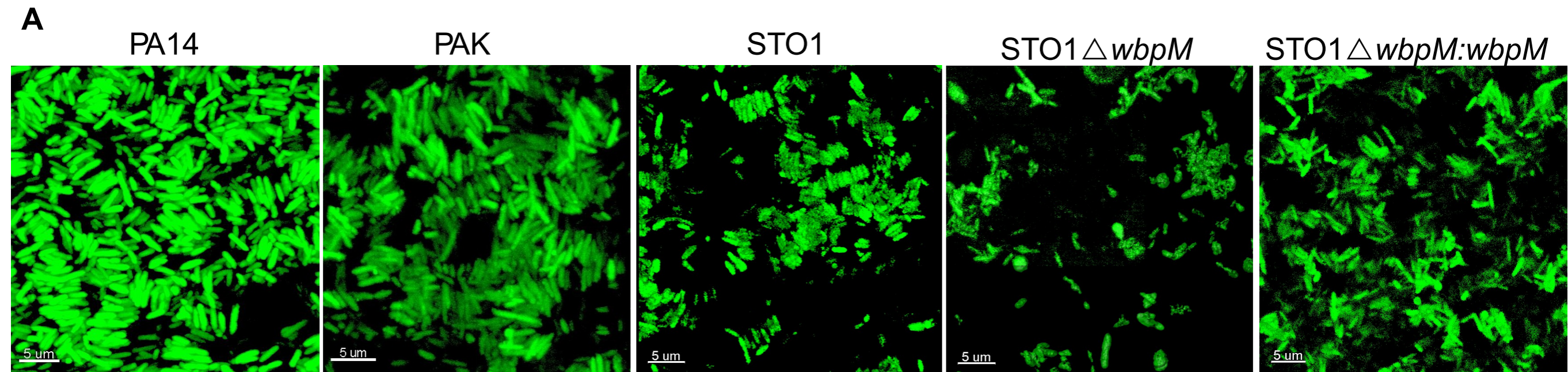


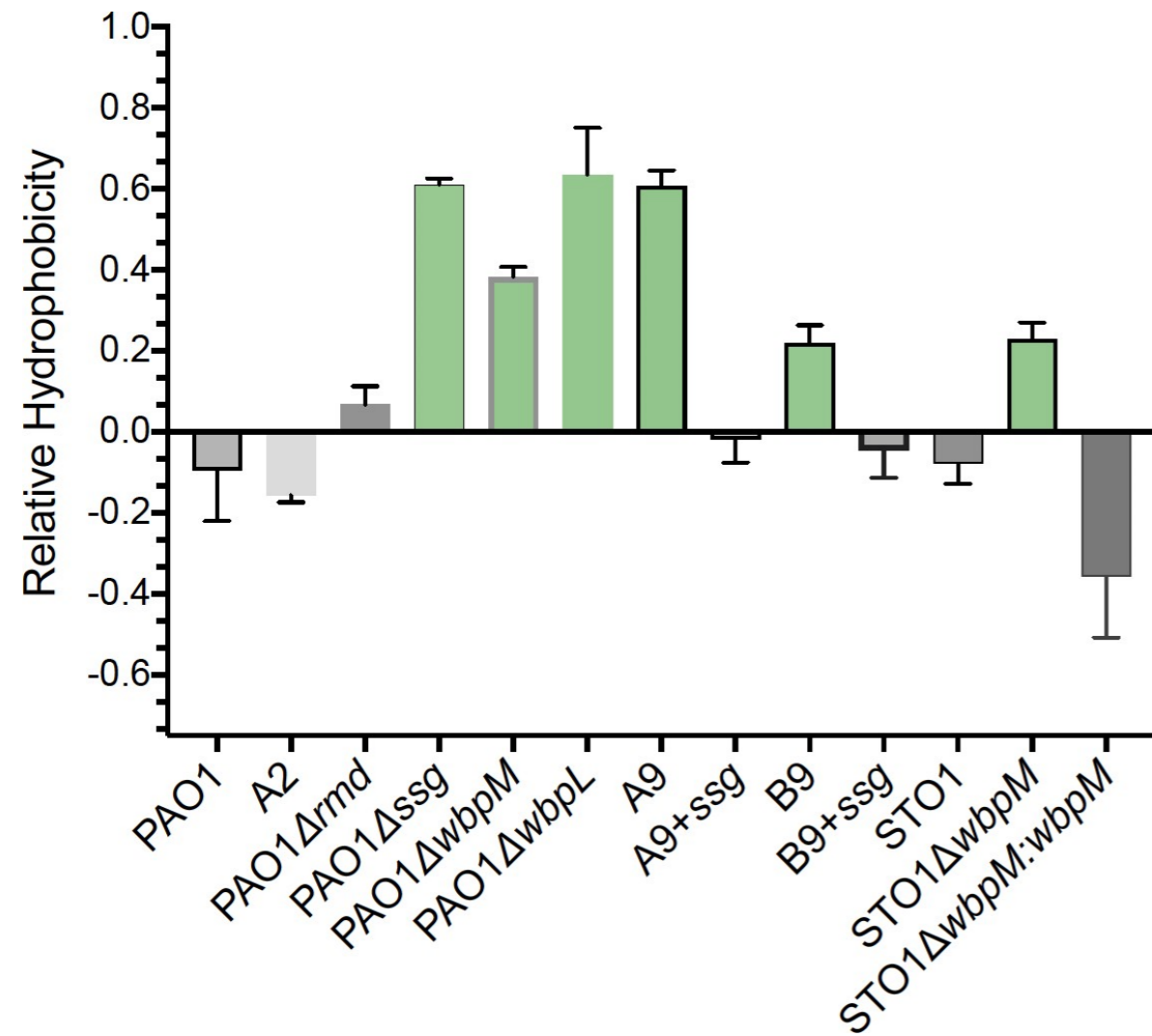
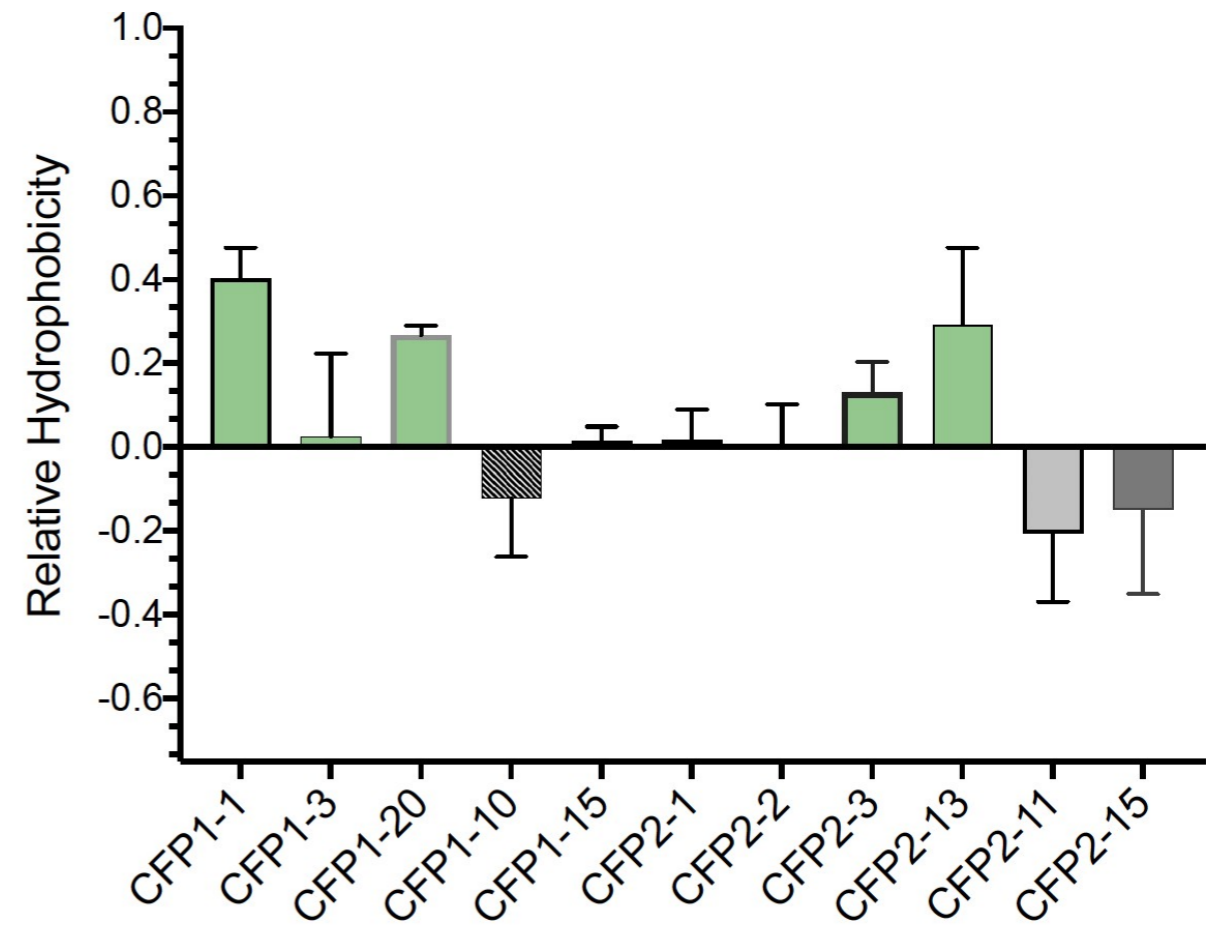
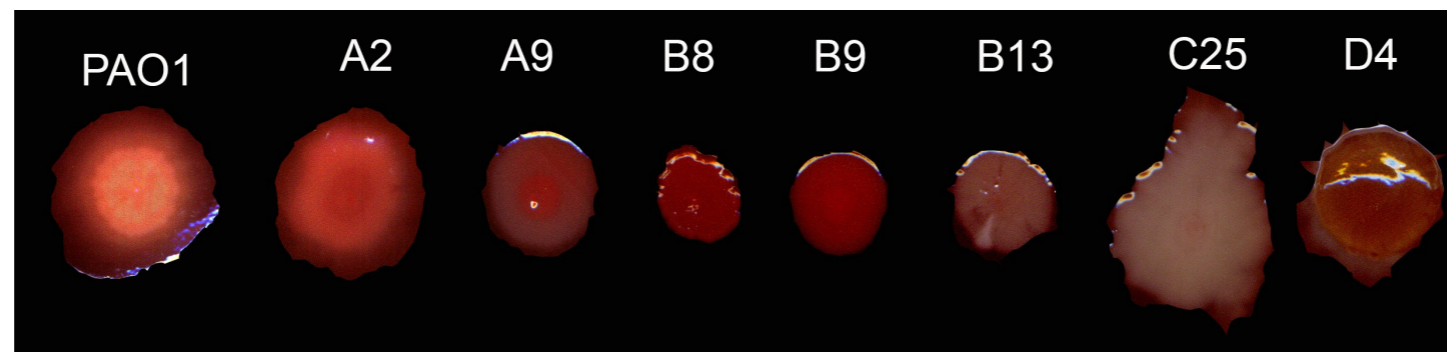
Figure 5**A****B**

Figure S1

available under aCC-BY 4.0 International license.

A



B

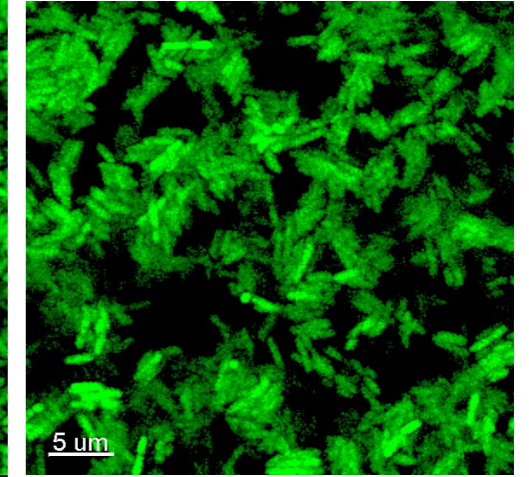
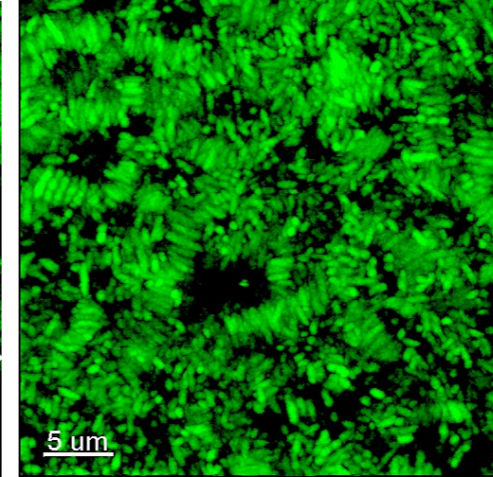
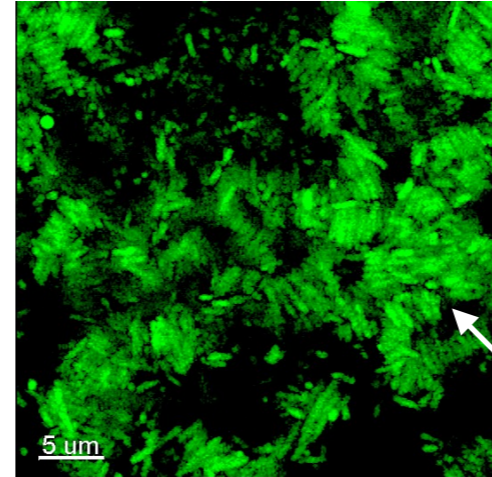
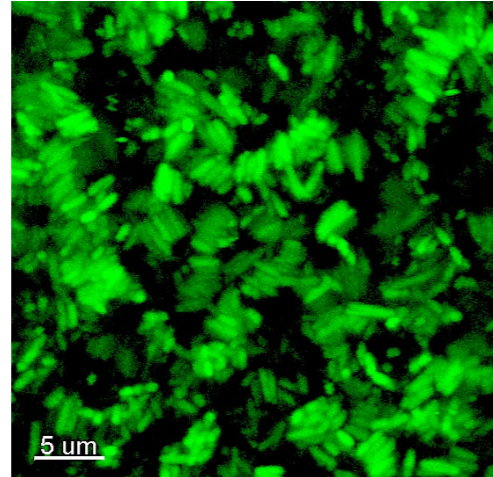
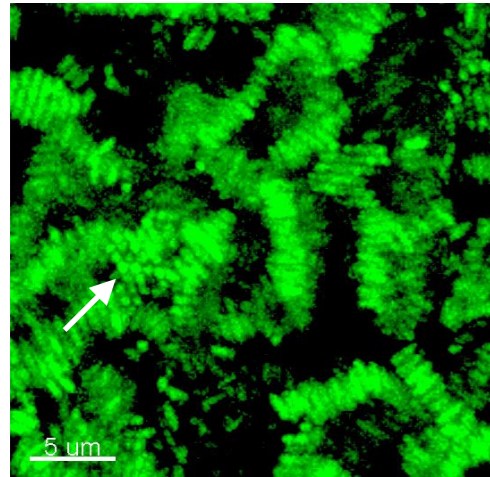
PAO1 (S)

B8 (S)

B13 (S)

C25 (S)

D4 (S)



C

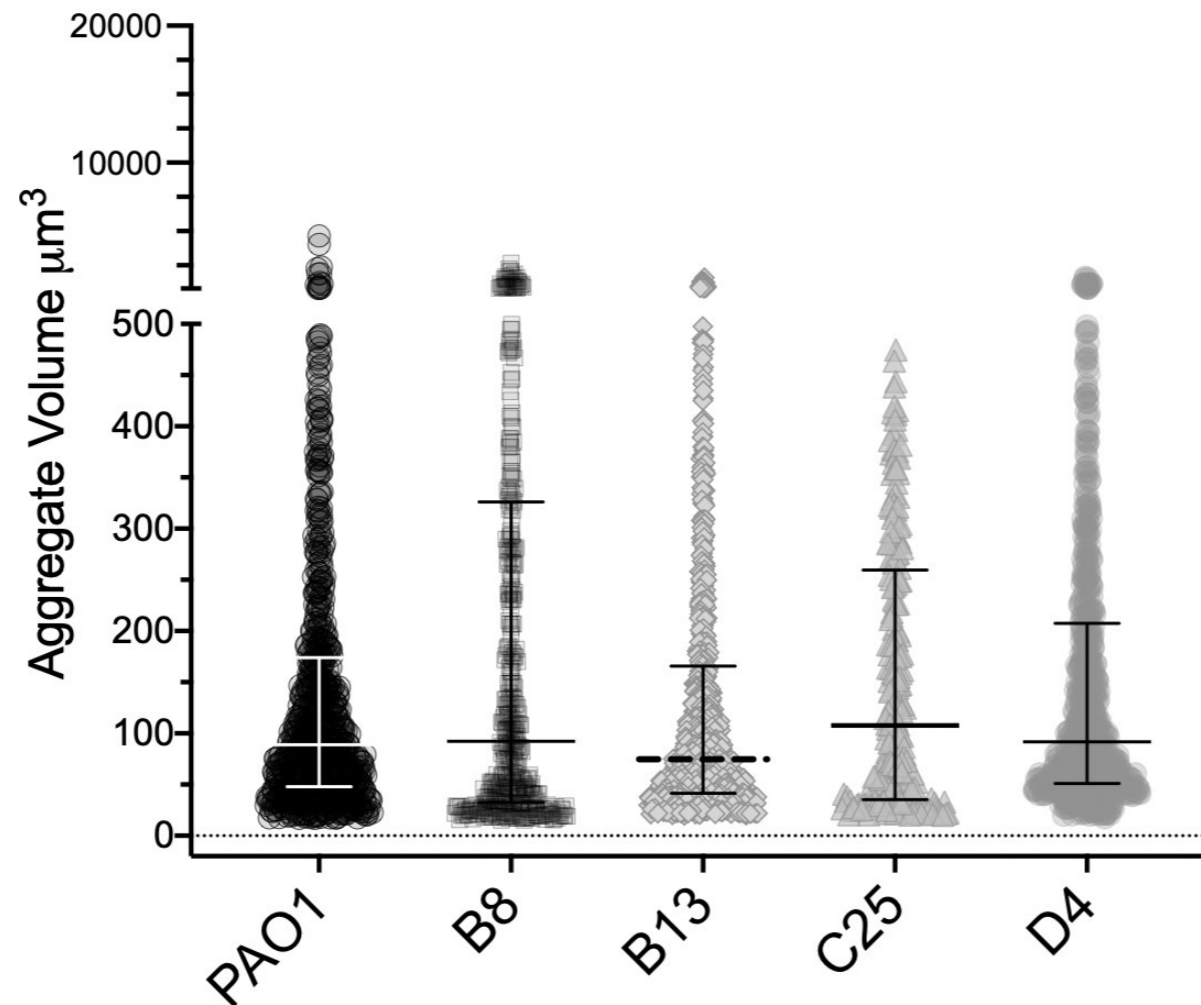


Figure S2

available under aCC-BY 4.0 International license.

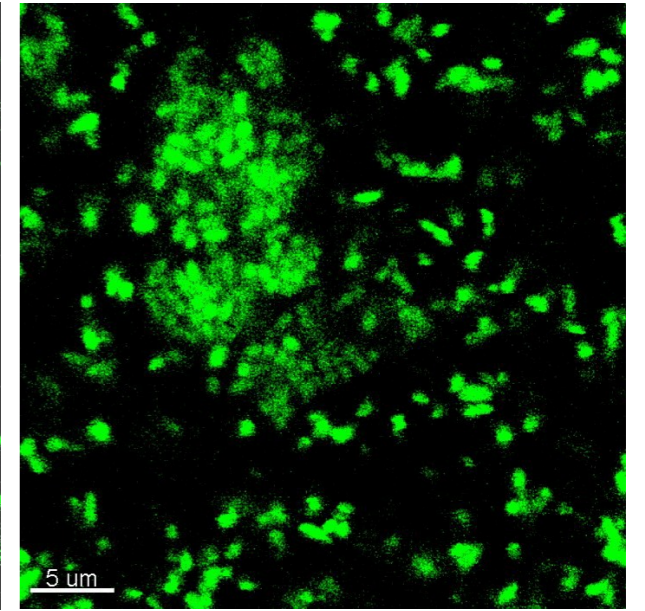
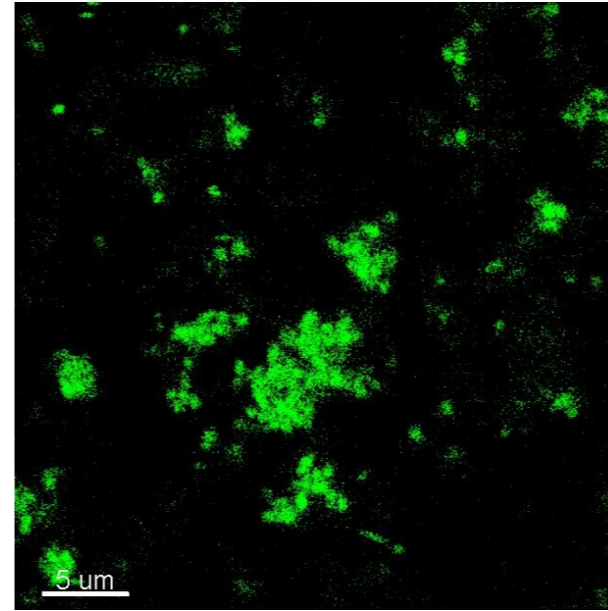
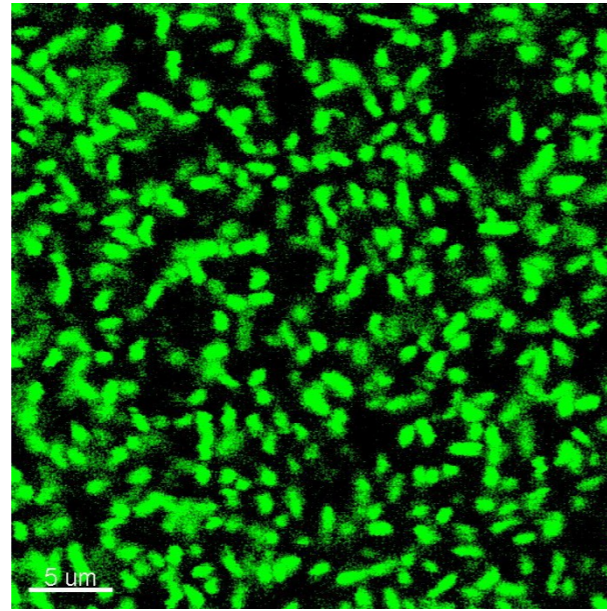
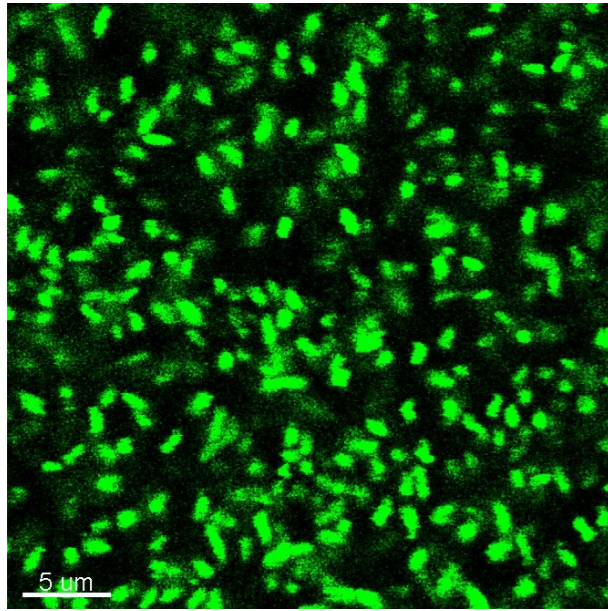
PAO1

A2

A9

B9

A



A9

A9+ssg

B9

B9+ssg

B

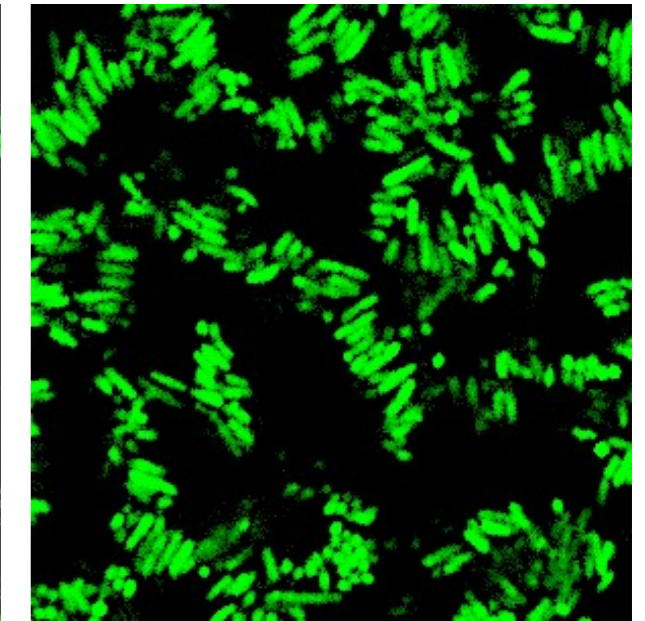
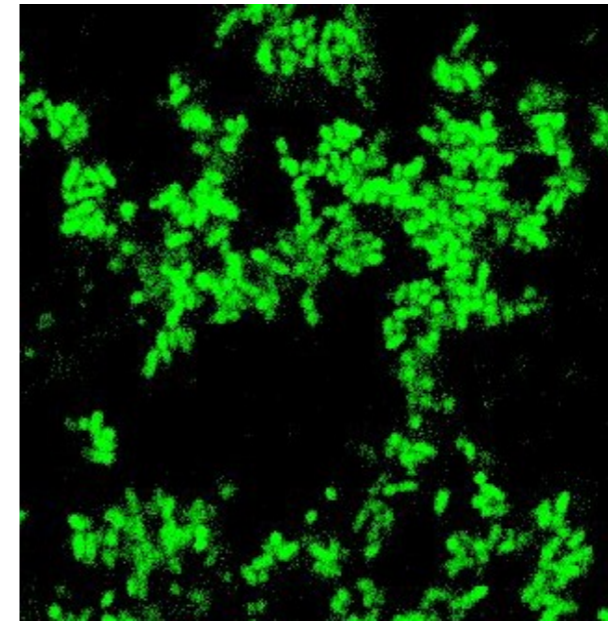
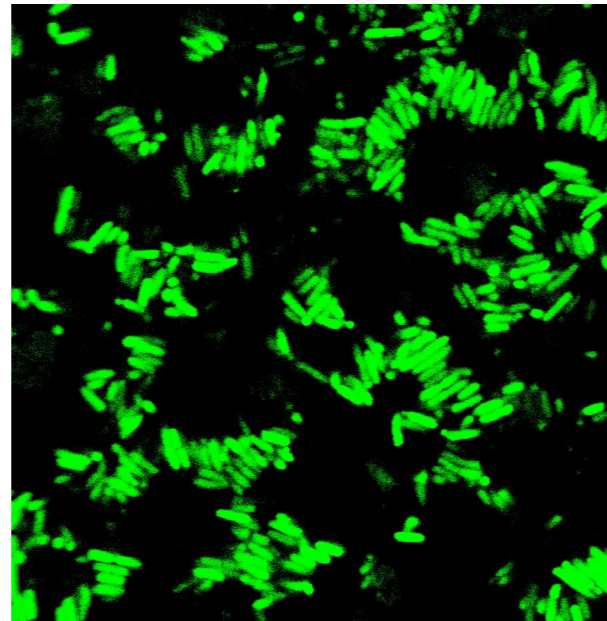
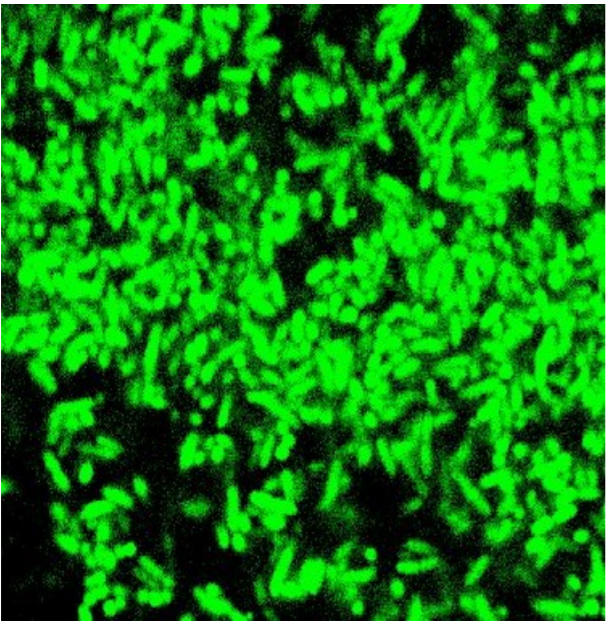


Figure S3

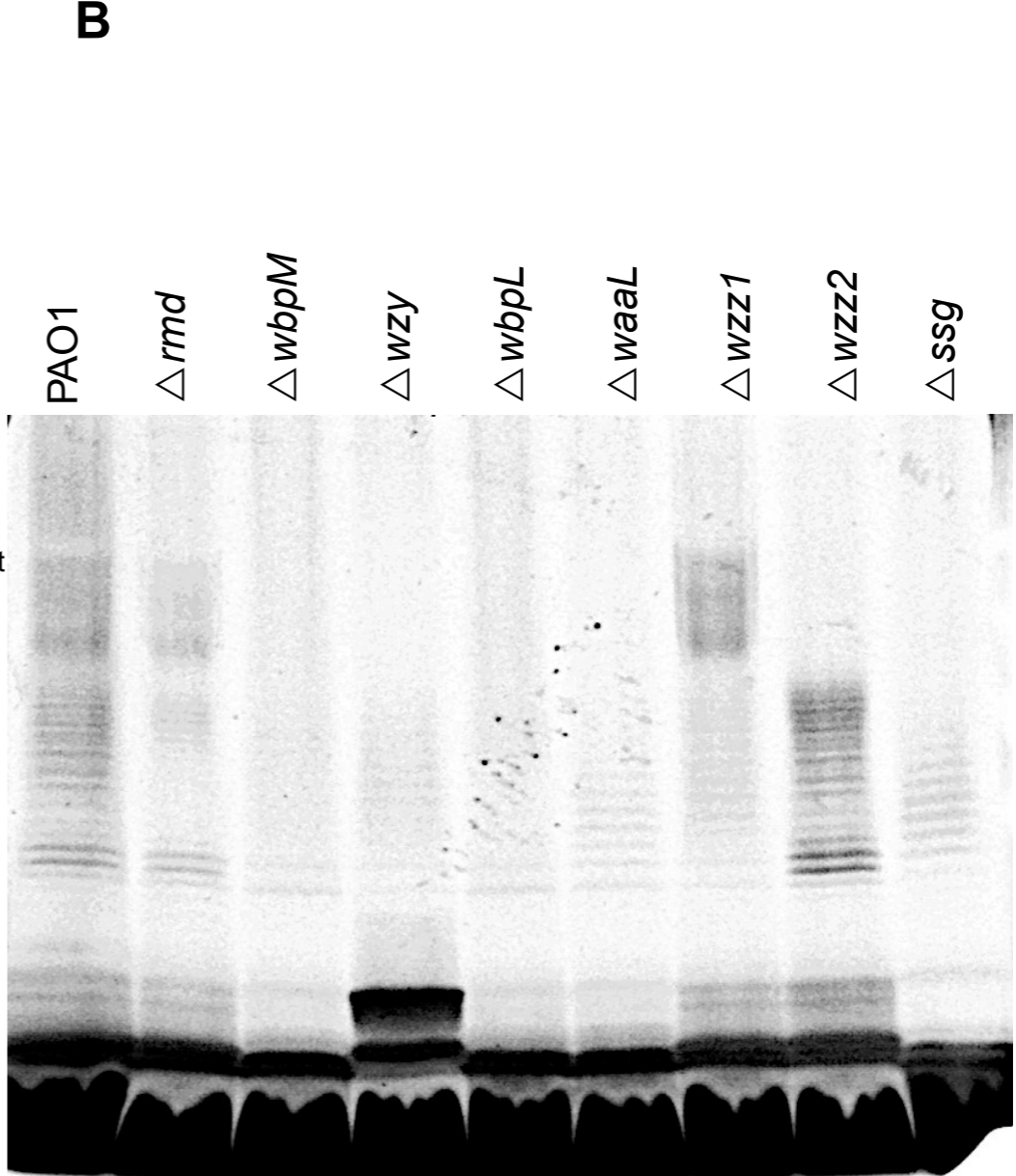
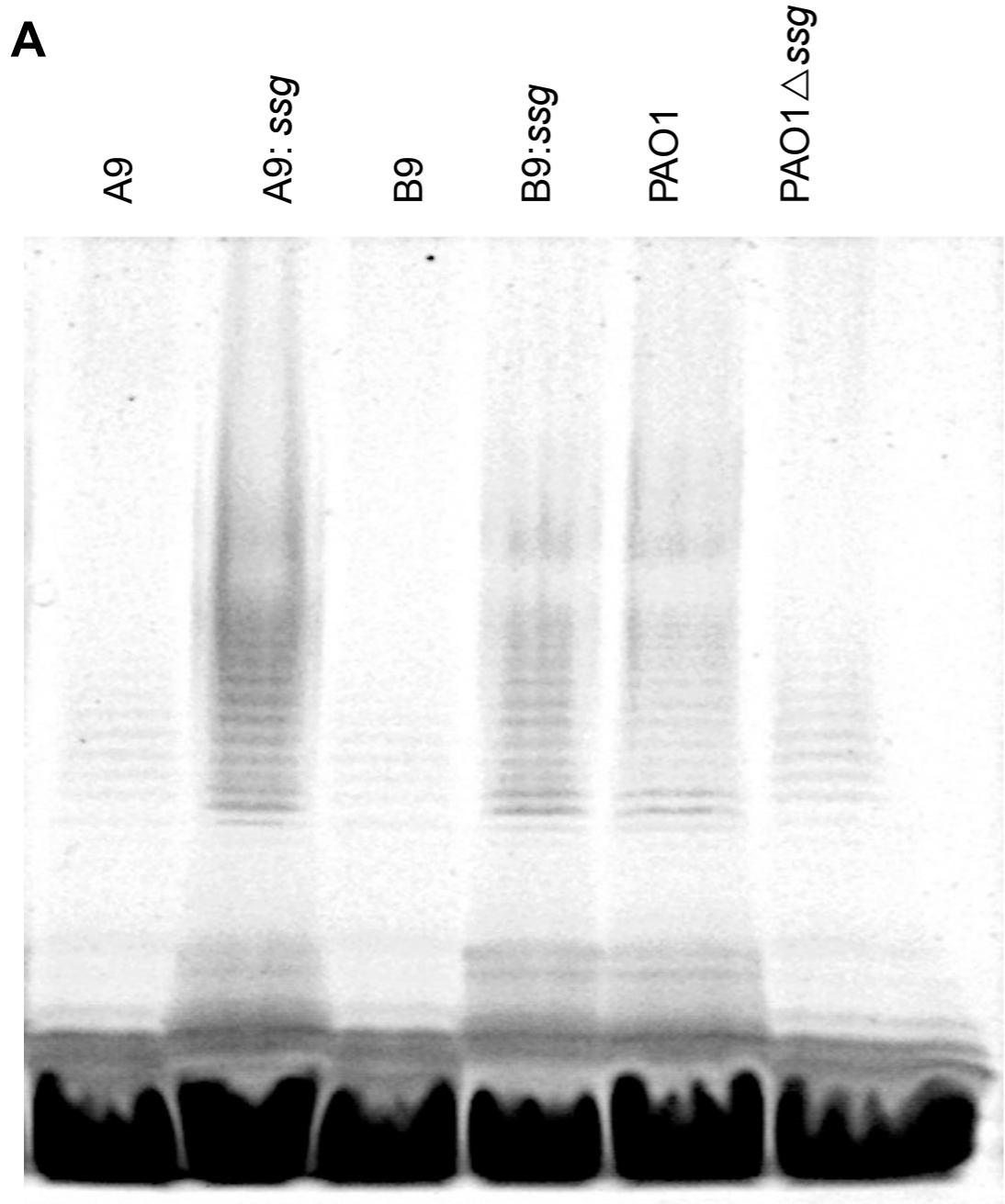


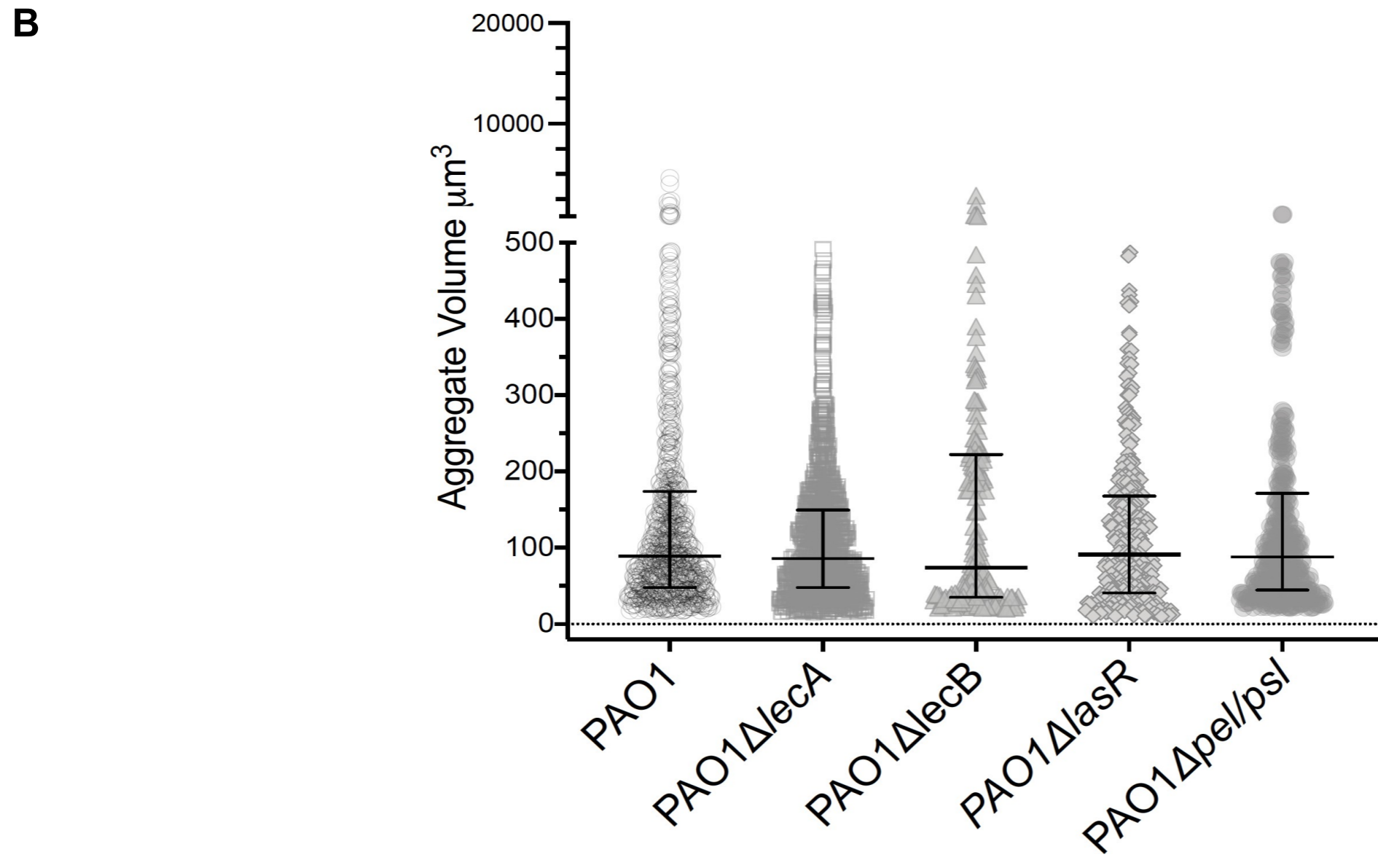
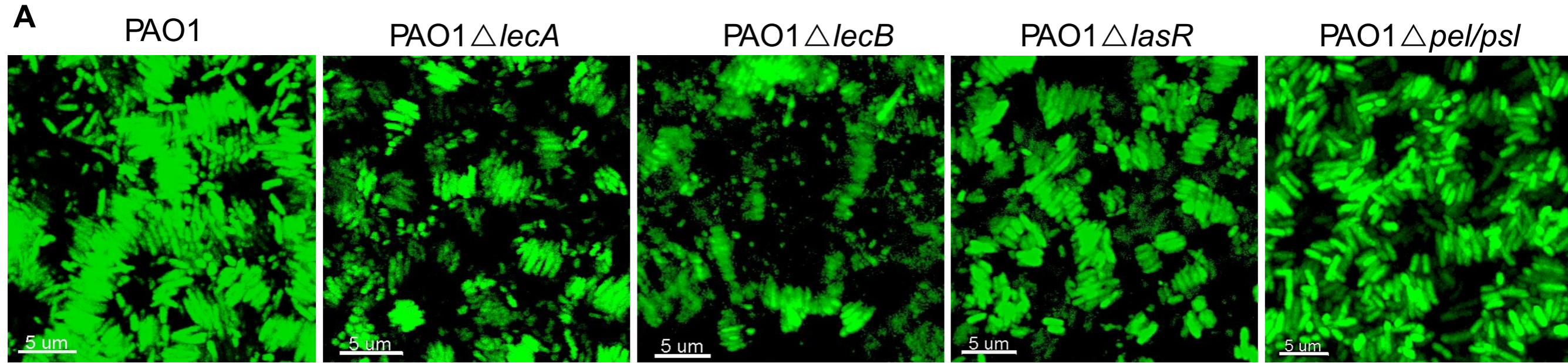
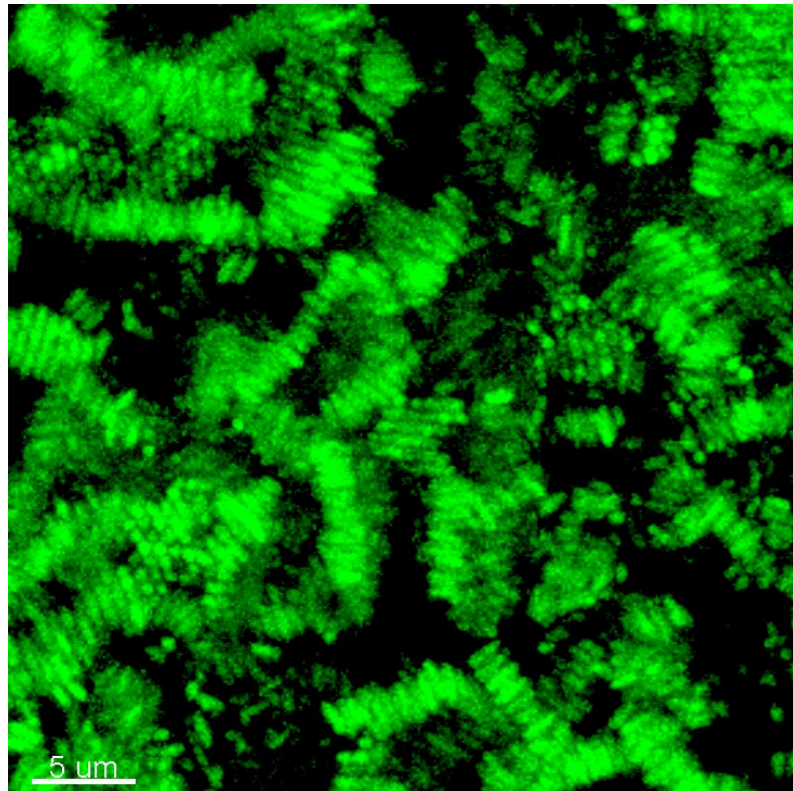
Figure S4

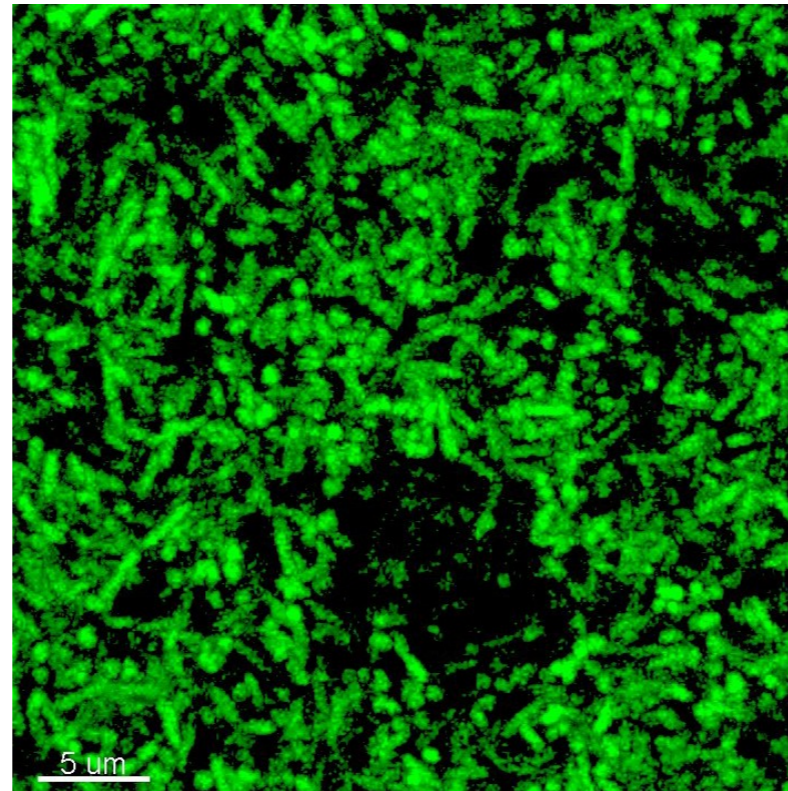
Figure S5

A

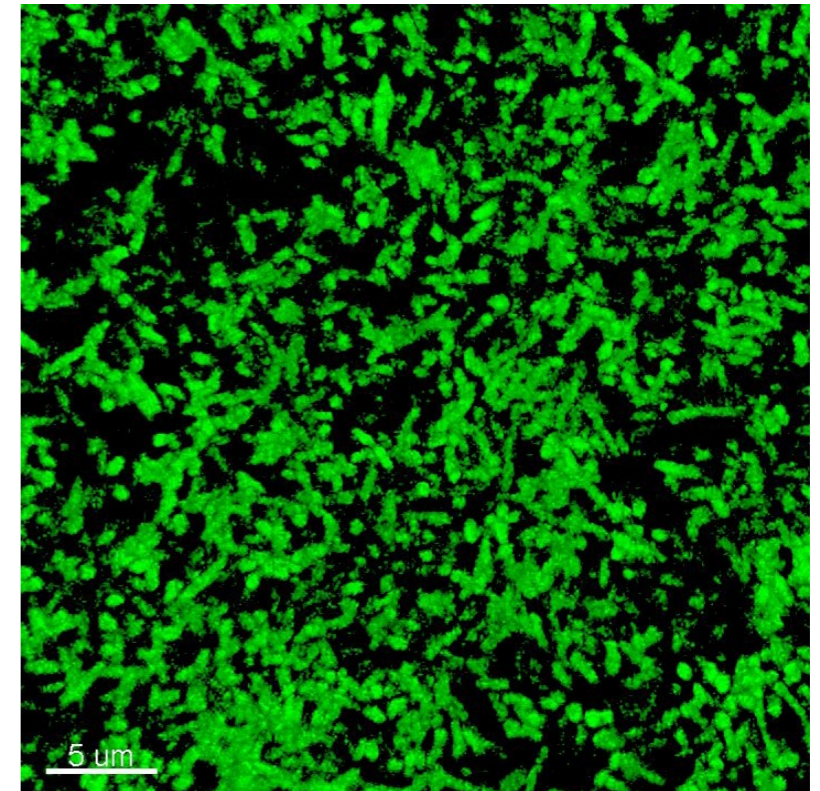
PAO1 (0.6 mg/ml DNA)
(5 mg/ml mucin)



PAO1 (0.12 mg/ml DNA)
(1 mg/ml mucin)

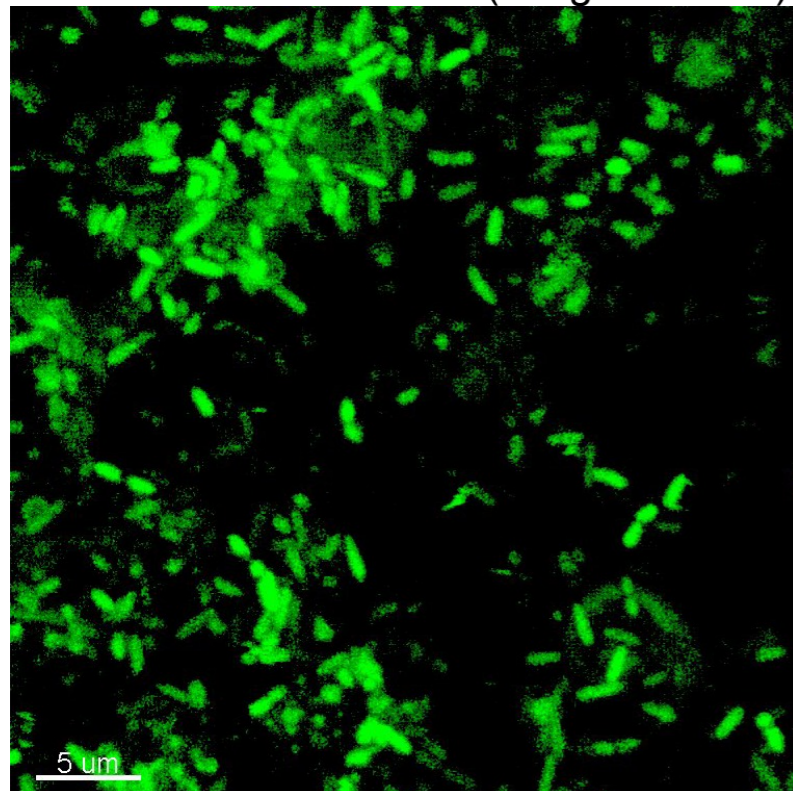


PAO1 (0.06 mg/ml DNA)
(0.5 mg/ml mucin)

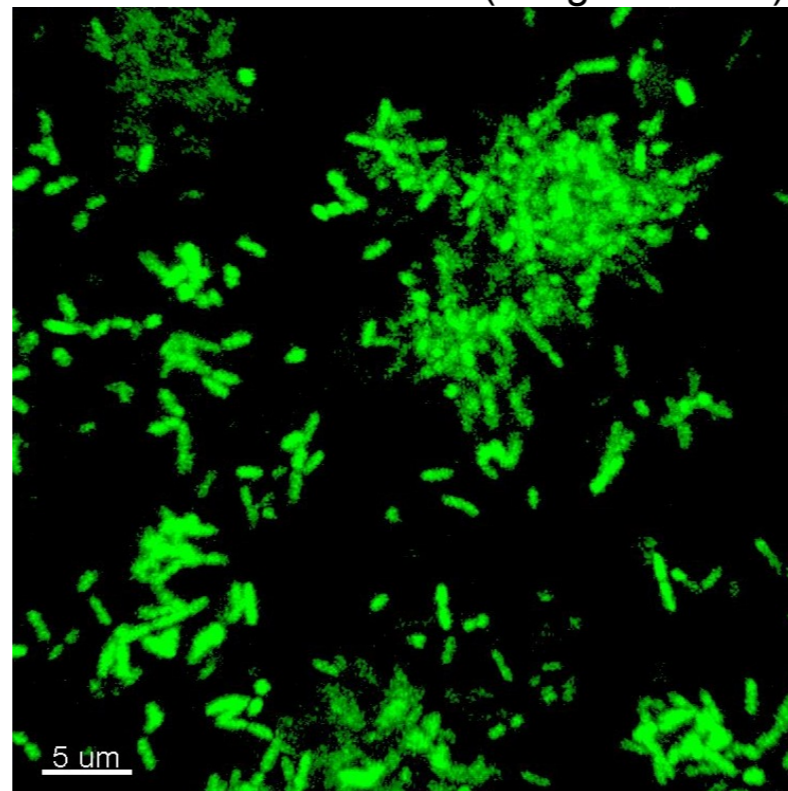


B

PAO1 $\Delta wbpL$ (0.6 mg/ml DNA)
(5 mg/ml mucin)



PAO1 $\Delta wbpL$ (0.12 mg/ml DNA)
(1 mg/ml mucin)



PAO1 $\Delta wbpL$ (0.06 mg/ml DNA)
(0.5 mg/ml mucin)

